quaternary

MDPI

Review

The Asian Summer Monsoon: Teleconnections and Forcing Mechanisms—A Review from Chinese Speleothem $\delta^{18}O$ Records

Haiwei Zhang [1,*], Yassine Ait Brahim [1], Hanying Li [1], Jingyao Zhao [1], Gayatri Kathayat [1], Ye Tian [1], Jonathan Baker [1], Jian Wang [1], Fan Zhang [1], Youfeng Ning [1], R. Lawrence Edwards [2,3] and Hai Cheng [1,2,*]

1 Institute of Global Environmental Change, Xi'an Jiaotong University, Xi'an 710054, China
2 Department of Earth and Environmental Sciences, University of Minnesota, Minneapolis, MN 55455, USA
3 School of Geography, Nanjing Normal University, Nanjing 210023, China
* Correspondence: zhanghaiwei@xjtu.edu.cn (H.Z.); cheng021@xjtu.edu.cn (H.C.)

Received: 21 March 2019; Accepted: 17 July 2019; Published: 23 July 2019

Abstract: Asian summer monsoon (ASM) variability significantly affects hydro-climate, and thus socio-economics, in the East Asian region, where nearly one-third of the global population resides. Over the last two decades, speleothem $\delta^{18}O$ records from China have been utilized to reconstruct ASM variability and its underlying forcing mechanisms on orbital to seasonal timescales. Here, we use the Speleothem Isotopes Synthesis and Analysis database (SISAL_v1) to present an overview of hydro-climate variability related to the ASM during three periods: the late Pleistocene, the Holocene, and the last two millennia. We highlight the possible global teleconnections and forcing mechanisms of the ASM on different timescales. The longest composite stalagmite $\delta^{18}O$ record over the past 640 kyr BP from the region demonstrates that ASM variability on orbital timescales is dominated by the 23 kyr precessional cycles, which are in phase with Northern Hemisphere summer insolation (NHSI). During the last glacial, millennial changes in the intensity of the ASM appear to be controlled by North Atlantic climate and oceanic feedbacks. During the Holocene, changes in ASM intensity were primarily controlled by NHSI. However, the spatio-temporal distribution of monsoon rain belts may vary with changes in ASM intensity on decadal to millennial timescales.

Keywords: ASM; SISAL; speleothem; oxygen isotope; paleoclimate; China

1. Introduction

The Asian summer monsoon (ASM) transports heat and moisture during boreal summer (JJA) across the Indian Ocean and the tropical western Pacific into the Indian subcontinent and southeastern Asia, extending as far as northeast China and Japan [1]. As the strength of the ASM directly influences the hydro-climate over these regions, its variability is of profound relevance to a large fraction of the world's population. The ASM system includes two interacting subsystems: the East Asian summer monsoon (EASM) and the Indian summer monsoon (ISM). Modern observations show that the ISM circulation and its associated moisture penetrate northeastwards, deep into East Asia and, as a result, the two subsystems cannot be clearly distinguished mechanistically [2]. China is influenced by both the EASM and ISM and, therefore, it is essential to study monsoon variability on various timescales to understand their global teleconnections, underlying forcing mechanisms, and, in turn, improve our ability to predict long-term trends of hydroclimatic change.

Speleothem records can be precisely dated using uranium-series disequilibrium dating methods [3,4], and several high-resolution climate proxies can be interpreted from their geochemistry (e.g., $\delta^{18}O$, $\delta^{13}C$, and trace-element ratios) [5–7]. Over the past two decades, a large number of high-resolution speleothem $\delta^{18}O$ records from China have been used to characterize ASM variability and its underlying mechanisms across the late Quaternary at different timescales [5,8–15]. As a result, China now has one of the highest densities of speleothem records (Figure 1).

The Speleothem Isotopes Synthesis and Analysis (SISAL) Working Group supported by Past Global Changes (PAGES) is an international effort to compile and synthesize stalagmite $\delta^{18}O$ and $\delta^{13}C$ records to explore past climate changes and enable climate model evaluation [16,17]. The first version of the database, SISAL_v1 [18] and database structure and content were described by Atsawawaranunt et al. [19]. An overview of the ISM evolution, as interpreted from speleothem records, has been published in this special issue by Kaushal et al. [20]. In this paper, we drew on SISAL_v1 to investigate climatic changes across China during the Late Quaternary. The database contains $\delta^{18}O$ and $\delta^{13}C$ data of stalagmites along with relevant age and cave information. Because the interpretation of Chinese $\delta^{13}C$ records is underdeveloped due to its complexity, we focused this review on available $\delta^{18}O$ records.

2. Cave Locations and Climatic Characteristics in China

The SISAL_v1 contains 64 speleothem records from 17 caves in China (Figure 1). These cave sites are mostly distributed in southern and central China, with fewer sites in northeastern and southeastern China. Although northwestern China and the Tibetan Plateau have well-developed karst systems (Figure 1), very few records have been published from these regions, such as the Kesang [21,22] and Baluk [23] caves in northwest China and the Tianmen [24,25] and Bengle [26] caves in Tibet. Difficulties with cave access, partly for religious concerns, have mainly contributed to the paucity of speleothem records from these areas. While significantly more stalagmite datasets have been published from southwestern China (i.e., Yunnan and Guangxi provinces), relatively low uranium concentrations tend to preclude their use for precise climate reconstructions. The most relevant records from this limestone-dominated region are from the Xiaobailong [13] and Dongge [8,12] caves in the southern part of southwestern China (Figure 1).

Currently, about one-fifth of the published speleothem $\delta^{18}O$ records in China have been incorporated into SISAL_v1. Geographically, most of the monsoon regions in China are adequately represented by these datasets (Figure 1). Hence, most studies highlight EASM variability on various timescales (Figures 1 and 2), as well as the relationship between palaeoclimate changes and Chinese culture and civilization [10,27–29]. For example, Kesang and Baluk cave records (NW China) shed light on the influence of the westerly jet and its possible linkages with the EASM, and the Tianmen and Bengle cave records (Tibetan Plateau) revealed a long-term variation in the ISM during the Holocene and Marine Isotope Stage (MIS) 5 [24–26] (Figures 1 and 2). Comas-Bru and Harrison [16] discussed the main reasons why some published speleothem records have not been included in SISAL.

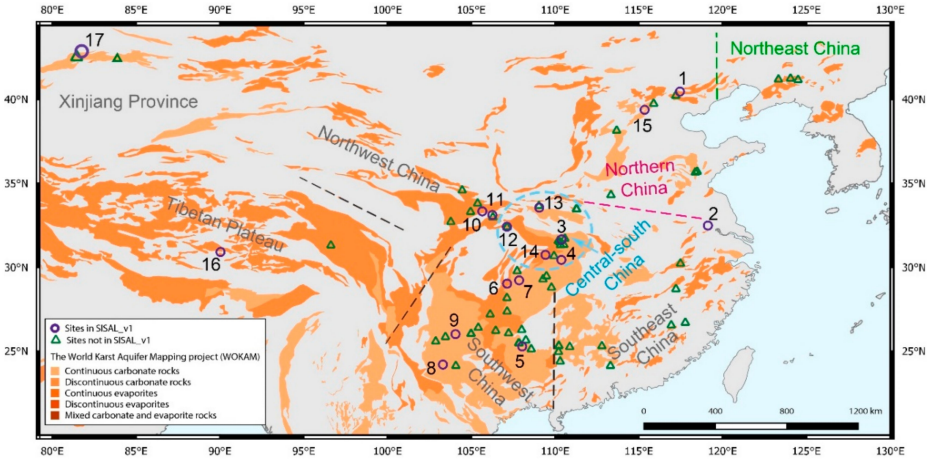

Figure 1. Map showing the location of speleothem records in China, superimposed on a map showing the distribution of carbonate and evaporite rocks provided by the World Karst Aquifer Mapping Project (WOKAM [30]). Purple circles indicate cave sites with speleothem records that are available in SISAL_v1 [18] (1: Kulishu; 2: Hulu; 3: Sanbao; 4: Heshang; 5: Dongge; 6: Yangkou; 7: Furong; 8: Xiaobailong; 9: Zhuliuping; 10: Huangye; 11: Dayu; 12: Suozi; 13: Jiuxian; 14: Xinya; 15: Xinglong; 16: Tianmen; 17: Kesang). Green triangles show cave sites identified, but not included in SISAL_v1.Specific information on sites, entities, and references is given in Table 1.

The EASM variability significantly affects hydro-climate across most of China, with two notable exceptions: (1) in NW China and the adjacent northern part of the Tibetan Plateau, where the westerly climate prevails; and (2) in SW China and the southern part of the Tibetan Plateau, where hydro-climate variability is mainly controlled by the ISM (Figure 2). Regions located around 110 °E are influenced by interactions between ISM and EASM (Figure 2). The EASM undergoes a meridional transition during its seasonal evolution, characterized by three quasi-stationary stages separated by two abrupt northward shifts in the frontal rainfall belt. Ding and Chan [31] summarized the meridional advance of the EASM as follows: (1) the first onset starts in early May, following the "spring persistent rainfall", is designated as the "pre-mei-yu" season; (2) in mid-June, the frontal rainfall abruptly shifts northwards, forming the Chinese "mei-yu"; and (3) the second abrupt shift occurs around mid-July, enhancing monsoon-associated rainfall over northern China. The conventional interpretation of the EASM seasonal evolution underlines the land–sea moisture-bearing thermal contrast caused by the differential heat capacities of the Asian continent and the Pacific Ocean, which induce a baroclinic contrast that drives a low-level monsoonal flow from South China Sea. However, Wang and Lin [32] suggested that the persistent spring rainfall over SE China is not related to the EASM, because the large-scale atmospheric circulation and rain-bearing systems differ from those associated with the typical summer monsoon frontal rainfall. Changes in EASM intensity are essentially reflected by the advance or retreat of the monsoon frontal rainfall belt, more northerly the penetration of the frontal rainfall belt, the greater the intensity of the EASM [33]. Recent publications suggest that changes in the timing and duration of the transition between EASM seasonal stages are linked to the north–south migration of the westerly jet relative to the Tibetan Plateau, with an early seasonal transition being associated to an early transition of the westerly jet [34]. The increase in insolation over the boreal summer reduces the latitudinal temperature gradient, leading to a weakened, northwardly shifted westerly jet. The meridional position of the westerlies relative to the Tibetan Plateau determines the onset of mei-yu and possibly the onset of the mid-summer stage. An earlier northward shift in the westerly jet triggers earlier seasonal rainfall transitions, and thus a shorter "mei-yu" and longer mid-summer stage [35].

During the summer monsoon season, precipitation occurs along a long trajectory (i.e., from more distal water sources). As a result, precipitation $\delta^{18}O$ values in eastern China become progressively lower, reaching their minimum during July–August [2]. This $\delta^{18}O$ minimum also coincides with

the maximum land–sea temperature contrast. During autumn, precipitation $\delta^{18}O$ values become progressively higher with the retreat of the summer monsoon. In contrast, boreal winter (DJF) precipitation $\delta^{18}O$ in eastern China exhibits a large spatial range in $\delta^{18}O$, with the lowest values in the north and highest values in the south. This meridional gradient likely results from the reversal of the predominant wind direction in association with the East Asian Winter Monsoon, driven rather by the eastern flank of the Siberian High [36], for which the "temperature effect" strongly determines regional meteoric $\delta^{18}O$ values [37]. Because winter precipitation contributes relatively little volume to the annual mean [2], spatial patterns in DJF precipitation $\delta^{18}O$ should generally have a negligible impact on speleothem $\delta^{18}O$ and, therefore, are less important to the interpretation of Chinese cave records. Overall, these observations demonstrate that seasonal precipitation $\delta^{18}O$ values are principally (and inversely) correlated with summer monsoon intensity and/or distance from moisture sources, which, in turn, is closely related to atmospheric circulation.

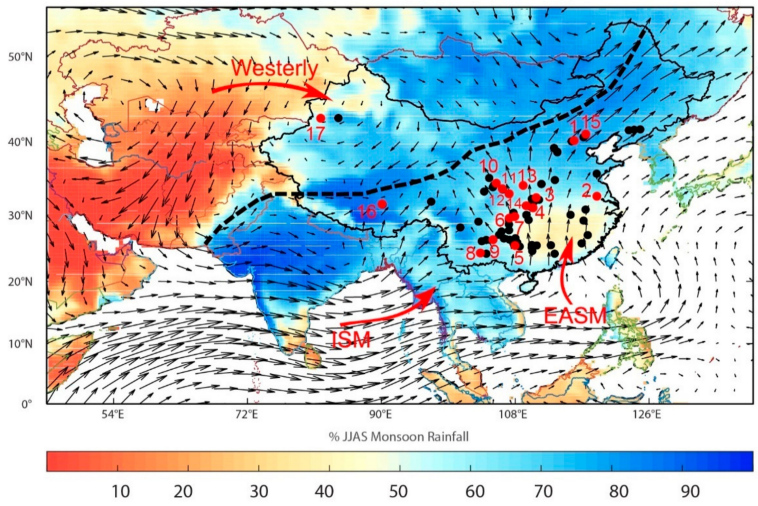

Figure 2. Long-term (1981–2010) percentage of summer precipitation (June–September) based on the 1.0° × 1.0° gridded gauge-analysis data from the GPCC (Global Precipitation Climatology Center [38]). Wind data at 850 hPa (June–September) are from MERRA (Modern-Era Retrospective analysis for Research and Applications [39]) database. Red and black dots are the locations of speleothem $\delta^{18}O$ records discussed herein (details in Table 1). Cave locations numbered 1–17 (red dots) are the same as in Figure 1. "EASM", "ISM", and "Westerly" denote regions mainly influenced by the East Asian summer monsoon, Indian summer monsoon, and Westerly climates, respectively. The regions located around 110° E represent the interaction area between ISM and EASM. The modern ASM limit is shown by the black, dashed line, as in Chen et al. [40]. Numbers indicate cave sites of records in SISAL_v1 (1: Kulishu; 2: Hulu; 3: Sanbao; 4: Heshang; 5: Dongge; 6: Yangkou; 7: Furong; 8: Xiaobailong; 9: Zhuliuping; 10: Huangye; 11: Dayu; 12: Suozi; 13: Jiuxian; 14: Xinya; 15: Xinglong; 16: Tianmen; 17: Kesang). See Table 1 for details of each record.

3. Chinese $\delta^{18}O$ Records in SISAL_v1

More than 200 speleothem $\delta^{18}O$ records from China have been published in the past two decades and SISAL_v1 contains 64 of these records from 17 caves. As discussed in Comas-Bru and Harrison (2109) [16], a range of challenges were faced at the time of compiling data for SISAL_v1 (e.g., large amounts of metadata missing) and efforts are being made towards incorporating the missing records in subsequent versions of the SISAL database. Nonetheless, most of the monsoon regions in eastern China are represented in SISAL_v1 with sufficient spatial representation to support our initial assessment (Figures 1 and 2). Future updates of the SISAL database will have a suitable spatial density to enable the investigation of spatio-temporal variations of the EASM and its interactions with the ISM and the westerly climate. Details on each speleothem $\delta^{18}O$ record and their status in the SISAL database are summarized in Table 1.

Table 1. Summary of Chinese speleothem records sorted alphabetically by site name. The records for which entity_ID is available are in SISAL_v1 [19]. Min/Max year BP correspond to the last/first stable isotope measurement of each record. BP is years before present, where present is 1950 CE. * indicates the papers published in Chinese journals.

Site_Name	Site_ID	Latitude ° N	Longitude ° E	Entity_Name	Entity_ID	Min. Year BP	Max. Year BP	Reference
Baigu		26.22	106.5	BG1		3300	12,800	[41] *
Baluk		84.73	42.43	BLK12A		2061	9308	[23]
				BLK12B		2698	8287	[23]
Bengle		31.32	96.66	14BL-1		388	3855	[26] *
Dark		27.2	106.17	D1		325	5486	[42]
				D2		1166	6127	[42]
Dashibao		26.08	105.05	DSB3		26,590	32,790	[43]
Dayu	36	33.13	106.3	DY-1	111	−33	720	[28,44]
Dongge	39	25.28	108.08	D3	114	91,200	163,500	[12]
				D8	324	217,202	225,258	[1]
				D4	115	116	148,400	[12]
				D4		−16.5	15,810	[45]
				DX1		800	2000	[46]
				DX2		1600	2000	[46]
				DAS		70	4200	[47]
				DA		−50	8880	[8,48]
				D15		0	885	[48]
				D4		130	15,470	[49]
Dongshiya		33.77	111.57	DSY1201		−62	139	[50]
				DSY1		−6	8700	[51]
Dragon		38.77	113.27	L30		1263.1	53,260	[52]
Dragon spring		25.65	108.3	L12		750	2000	[53]
				L12		9000	9600	[53]
E'mei		29.5	115.5	EM1		−59	140	[54]
Fengyu		24.5	110.33	F-1		4397	64,930	[55]
				F-4		−50	653	[49,55]
Furong	80	29.23	107.9	FR-5	171	6001.4	16,991	[56]
				FR-0510	172	−55	1989	[57]
Golden lion		25.12	108.62	JSD-01		87,900	88,200	[53]
				JSD-02		93,800	95,200	[53]
Haozhuzi		30.68	109.98	HZZ11		9000	30,000	[14,58]
				HZZ27		9000	53,000	[14,58]
Heizhugou		28.56	103.05	EB1		140	500	[59] *
Heilong		31.67	110.43	BD		170	1090	[60]
Heshang	122	30.45	110.42	HS4	253	−52	9470	[15]
				HS4	254	8061	8295	[61]
Huanglong		32.72	103.82	HL021		1951 CE	2002 CE	[62]
				HL022		1951 CE	2002 CE	[62]
Huangye	17	33.58	105.12	HY1	76	−32	1190	[63]
				HY2	77	1073	1812	[63]
				HY3	78	−51.8	642	[63]
Hulu	6	32.5	119.17	MSD	40	18,310	53,001	[5,64]
				MSL	41	35,900	75,646	[5,64]
				PD	42	10,495	19,338	[5]
				YT	43	14,389	17,234	[5,65–67] *
				H82	44	10,540	22,100	[5,68]
				HL162		134,511	159,096	[69]
				MSP		133,130	154,970	[70]
				MSX		128,030	154,520	[70]
				MSH		161,720	178,050	[70]
				H98		21,345	24,124	[71–73] *
Jintanwan		29.48	109.53	J1		11,000	12,900	[74]
				J1		14,700	29,500	[74]
Jiuxian	154	33.57	109.1	C996-1	329	−48	8614	[75]
				C996-2	330	−8	18,958	[75]
Kaiyuan		35.72	118.53	KY1		58	733	[76]
Kesang	2	42.87	81.75	KS06-A-H	11	3570	9890	[21]
				KS06-A	12	53,270	235,118	[21]
				KS06-B	13	257,190	456,456	[21]

Table 1. *Cont.*

Site_Name	Site_ID	Latitude ° N	Longitude ° E	Entity_Name	Entity_ID	Min. Year BP	Max. Year BP	Reference
				KS08-1-H	14	5	3520	[21]
				KS08-1	15	75,375	298,325	[21]
				KS08-2-H	16	8429	15,009	[21]
				KS08-2	17	70,873	230,103	[21]
				KS08-2-MIS3	18	51,607	53,727	[21]
				KS08-6	19	852	1318	[21]
				CNKS-2		235	1098	[22]
				CNKS-3		130	1158	[22]
				CNKS-7		2523	71,710	[22]
				CNKS-9		−71	73,551	[22]
Kulishu	45	39.68	115.65	BW-1	121	10,378	13,971	[77,78]
Laomu		33.77	111.56	LM1		257,000	324,000	[79] *
				LM2		8439	10,947	[51]
Lianhua (Hunan)		29.48	109.53	LHD1		−61	402	[80]
				LHD5		8030	11,918	[81]
Lianhua (Shanxi)		29.48	109.53	LH4		229	14,594	[82]
				LH5		1444	4176	[82]
				LH9		229	14,594	[82]
Linyi		35.68	118.42	LY		11,400	16,400	[83]
Linzhu		31.52	110.32	LZ15		224,630	348,950	[11]
				LZ36		348,850	361,880	[11]
Longquan		25.48	107.87	LQ2		200	1550	[84] *
Longfugong		31.72	110.78	LFG21		10,687.4	12,457.6	[85] *
Magou		34.32	113.38	MG-1		4900	13,100	[86] *
				MG-40		7100	13,100	[86] *
Maomaotou Dayan		25.31	110.27	DY-2		−59	−18	[87] *
Niudong		31.7	110.27	N1		82	9888	[88]
Nuanhe		41.33	124.92	NH5		4210	10,144	[89,90] *
				NH12		374	1057	[89,91] *
				NH13		1167	4729	[89] *
				NH20		1720	7804	[89] *
				NH33		7748	8638	[92] *
				NH6		7050	8630	[93] *
				NH7		200	3500	[91] *
Panlong		24.96	110.25	PL-1		0	36,400	[94] *
Qingtian		31.33	110.37	QT9		6100	6700	[95,96] *
Qingtian		31.33	110.37	QT20		16,105	17,564	[96,97] * [98]
				QT29		17,890	18,216	[97] * [98]
				YT		14,400	18,300	[97] *
				QT		12,080	13,480	[99]
				QT16		10,850	13,420	[100,101] *
				QT33		4840	5570	[102] *
				QT15		29,400	27,400	[103] *
				QT17		12,100	13,500	[104] *
				QT24		7362	7748	[105]
				QT40		7625	8782	[101] [105,106] *
				QT41		6507	7378	[105]
				QT9		6082	7020	[105]
				QT25		7297	10,832	[105]
				QT1		22,412	28,659	[107]
Qixing		26.07	107.27	QX-1		150	7700	[108]
				QX3		50	2312	[109] *
				Q4		12,400	44,330	[110,111] *
				Q6		11,290	59,680	[110,111] *
				Q1		65,900	85,500	[110,111] *
				Q2		38,500	60,400	[110,111] *
				QX1		2284	3574	[112]
Sanbao	140	31.67	110.43	SB-10	295	2089	11,532	[113] [114,115] *
				SB-6		1273	3243	[116] *
				SB-22		56,600	95,000	[115,117] *
				SB-25		78,100	132,500	[115,117] *
				SB-60		240,000	284,000	[118]
				SB-46		16,930	32,300	[43]

Table 1. *Cont.*

Site_Name	Site_ID	Latitude ° N	Longitude ° E	Entity_Name	Entity_ID	Min. Year BP	Max. Year BP	Reference
Sanbao	140	31.67	110.43	SB-26	296	403	5229.12	[116] * [113]
				SB-27	297	2351	8475.98	[116] * [113]
				SB-43	298	70	12,863	[113]
				SB-44	299	6860	13,179	[113]
				SB-49	300	10,206	13,185	[113]
				SB3		11,100	17,700	[115] *
				SB11		129,300	184,500	[115] *
				SB23		98,900	127,200	[115] *
				SB24		155,500	182,400	[115] *
				SB34		103,600	109,400	[115] *
				SB41		108,100	138,200	[115] *
				SB42		133,700	167,600	[115] *
				SB-12	301	424,300	462,800	[1]
				SB-14	302	299,200	624,400	[1]
				SB-32	303	503,800	641,300	[1]
				SB-58	304	426,300	464,900	[1]
Sanxing		27.37	107.18	SX7		86,600	108,200	[119]
				SX24		92,800	103,700	[119]
				SX29		106,300	113,500	[119]
				SX2		30,900	11,200	[120]
				SX3		3500	9700	[120]
				SX3		11,600	12,500	[120]
				SX5		14,900	17,500	[120]
				SX10		75,740	78,949	[121]
				SX16		68,774	77,001	[121]
Shennong		28.71	117.26	SN17		3643	5300	[122]
				SN4		−53	2500	[123]
				SN20		−53	2200	[123]
				SN3		8138	9239	[124]
				SN15		5617	7526	[124]
Shigao		28.18	107.17	SG1		4171	9811	[125,126] *
				SG2		209	5663	[125]
Shihua		39.78	115.93	TS9501		665 BC	1985 CE	[127]
				XMG-1		−65	80	[128]
				S312		1520 CE	1994 CE	[129]
				TS9701		200 BC	2000 CE	[130]
				LS9602		1000 CE	2000 CE	[130]
Shizi		32.4	107.17	SI3		46,000	54,000	[131] * [132]
Shuinan		25.33	110.27	SU		147,900	245,200	[133] *
Shuidong		41.28	124.1	TW9801		139	929	[134]
Songjia		32.41	107.18	SJ1		14,000	43,000	[135] *
				SJ3		14,800	19,800	[136,137]
				SJ5-6		320,000	334,000	[138] *
Suozi	59	32.43	107.17	SZ2	143	102,810	119,340	[139] * [140]
Tangshan		32.06	119.04	996182		10,500	16,800	[141]
Tianmen	142	30.92	90.07	TM-2	306	76,398	125,146	[24]
				TM-5	307	123,227	127,215	[24]
				TM-18a	308	4148	9045	[25]
				TM-18b	309	611	1026	[25]
Tian'e		31.72	110.37	TE2		590	2100	[142] *
				SW4		22,000	28,500	[107,143] *
				SW5		26,500	33,852	[107]
				SL		11,670	22,200	[143] *
				SW12		58,810	76,100	[144] *
Wangjiawei		41.22	123.38	W6		5848	8082	[145]
				W4		5069	10,269	[145]
Wanxiang		33.32	105	WX42B		−53	1758	[10]
				WXB07-4		4920	6420	[27]
Wulu		26.05	105.03	Wu3		29,220	39,170	[146]
				Wu32		20,800	29,000	[43]
				Wu23		26970	59,800	[147,148] * [149]
				Wu26		51,560	61,190	[147,148] * [149]
				Wu30		33,852	50,521	[107]
Wuya		33.82	105.42	WY27		1641 CE	2010 CE	[150]
				WY33		1749 CE	2011 CE	[150]

Table 1. *Cont.*

Site_Name	Site_ID	Latitude ° N	Longitude ° E	Entity_Name	Entity_ID	Min. Year BP	Max. Year BP	Reference
Xianglong		33	106.33	XL16		653	4291	[151]
				XL2		1972	4200	[151]
				XL26		2984	6651	[151]
				XL15		10,900	25,500	[152]
Xiangshui		25.25	110.92	XU		3800	6000	[153]
				X1		3100	44,000	[94] *
				X1		490	6000	[49]
Xianren		24.12	104.12	YPXR-5		192	292	[154]
Xianren		25.85	103.5	XR1		2100	7985	[155,156] *
Xianren		27.76	100.6	LX1		2100	4200	[157] *
Xianyun		25.55	117	XY III-28		26,330	22,980	[158] *
				XY IV-3		15,200	16,800	[159]
Xiaobailong	127	24.2	103.35	XBL-1		36,000	53,000	[160]
				XBL-3	263	30,140	41,420	[13]
				XBL-4	264	57,418	81,951	[13]
				XBL-7	265	59,670	71,000	[13]
				XBL-26	266	73,060	251,960	[13]
				XBL-27	267	172,340	189,460	[13]
				XBL-29	268	5340	43,630	[13]
				XBL-48	269	76,610	106,540	[13]
				XBL-65	270	167,250	170,730	[13]
Xinglong	69	40.5	117.5	XL-1	153	50,137	56,834	[161]
Xiniu		31.35	110.57	SN		180	2220	[162] *
Xinya	112	30.75	109.47	XY-2	221	57,617	69,553	[163]
				XY07-8	222	−55.46	3944.47	[164]
Yamen		25.48	107.9	Y1		73,000	162,000	[165]
Yangkou	5	29.03	107.18	YK5	34	179,643	190,358	[166]
				YK12	35	133,508	181,866	[166]
				YK23	36	172,620	206,839	[166]
				YK47	37	129,990	132,020	[166]
				YK61	38	95,506	173,089	[166]
				JFYK7	39	37,793	78,874	[167–169]
Yangzi		29.78	107.78	Y02		65,000	90,000	[170,171] *
Yelang		26.04	105.74	YLD15		−58	700	[172]
				YLD15		4500	5800	[172]
				YLD15		7400	13,400	[172]
				YLD15		33,700	35,050	[172]
Yongxing		31.58	111.23	NO.YXB		243,400	250,100	[173]
				YX92		1780	1960	[174] *
				YX46		61,620	87,330	[173]
				YX51		22,320	57,270	[173,175] *
				YX55		29,610	64,460	[173]
				YX15		279,000	322,600	[176]
				YX21		127,320	124,950	[177] *
Yuhua		26.7	117.82	YH1		−59	477	[178] *
Zhuliuping	174	26.02	104.1	ZLP1	379	4620	10,395	[179]
				ZLP2	380	9447	14,659	[179]
Zhenzhu		38.25	113.7	ZZ12		−50	800	[180]

The temporal distribution of the Chinese stalagmite $\delta^{18}O$ records in SISAL_v1 (Figure 3) spans a wide range of timescales. Multiple records provide information on glacial–interglacial and orbital timescales, such as the composite speleothem $\delta^{18}O$ record from Hulu [5], Sanbao [9], and Linzhu [11] caves in central–south China. This is the longest speleothem-based record published (it covers the full U–Th dating range [1]) and provides a 640 kyr record of EASM variability on orbital to millennial timescales [1]. The Kesang cave record is sensitive to changes in the westerly climate from NW China and spans from the Late Holocene to 500 kyr BP [21]. In SW China, the composite $\delta^{18}O$ record from the Xiaobailong Cave presents a 252 kyr record that has been linked to ISM variability and its interaction with the EASM [13]. The sampling resolution of these longer records varies from ~5 to 1300 years (Figure 3). More than ten $\delta^{18}O$ records capture the last interglacial period, though with large variance of temporal ranges and age constraints (Figure 3). Six of these have a temporal resolution between 6 and 240 years and a precise age control (Figure 3). This enabled an in-depth characterization of the last glacial EASM variability, especially at the millennial time-scale, and of abrupt changes such as Dansgaard/Oeschger and Heinrich events [5,9,43,120,146,173]. The highest temporal resolutions are found in the Holocene, with some records having a resolution between 1 to

20 years [8,15,25,45,51,75,81,82,108,113,125,151,153] (Figure 3). Figure 4 shows the spatial distribution of speleothem $\delta^{18}O$ records in China during three periods: the Late Pleistocene (640 ka–11.7 ka), the Holocene (11.7 ka–Present), and the last 2000 years. These datasets are broadly distributed across China and suggest a heterogeneous spatio-temporal distribution of precipitation or monsoon changes.

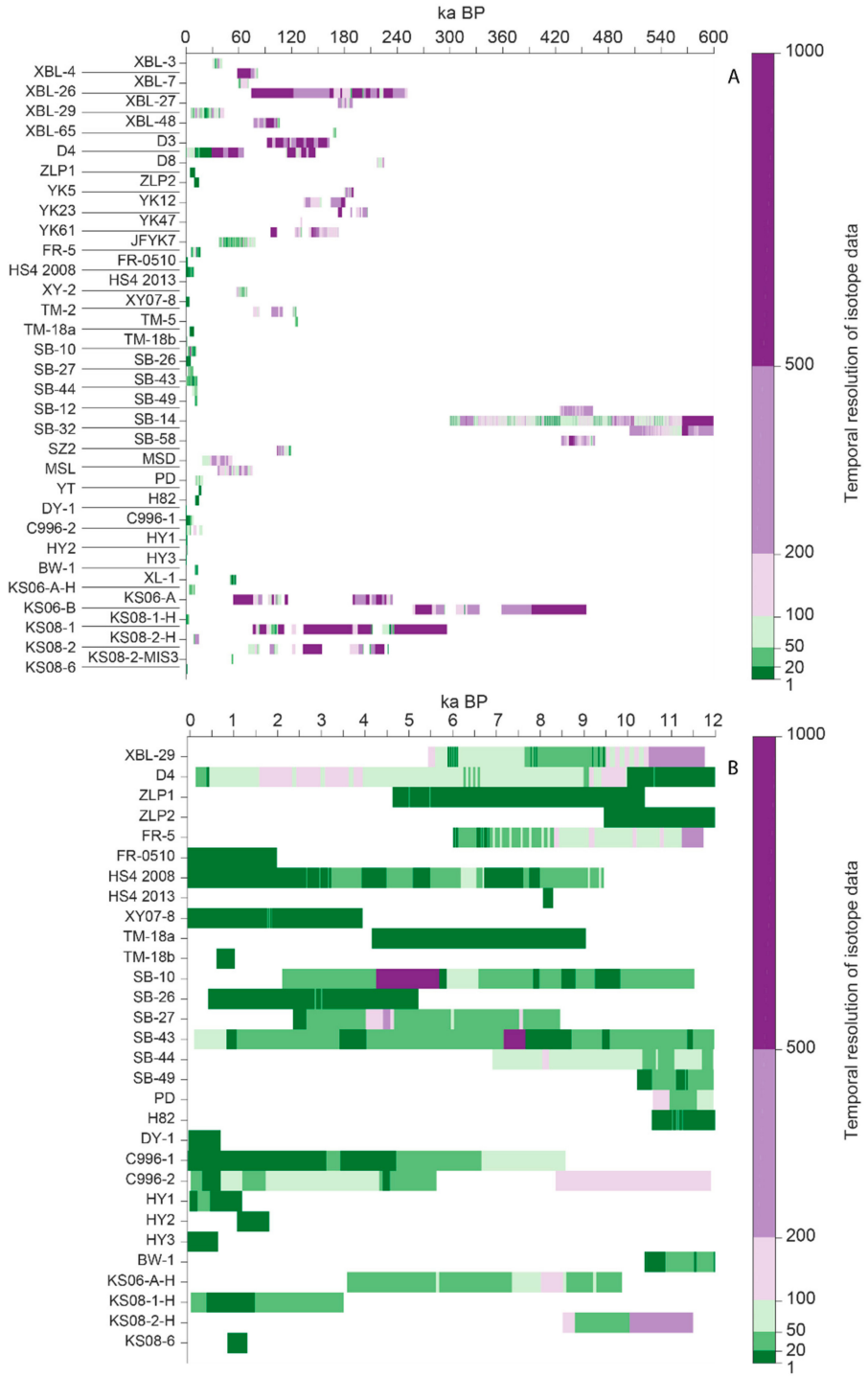

Figure 3. Temporal distribution of stalagmite $\delta^{18}O$ records from China in SISAL_v1 [19]. Panel (**A**) shows all available records and panel (**B**) focuses on the last 12 kyr. The color bar represents the temporal difference among consecutive isotopic samples in years. Labels on the *y*-axis are the entity_names as in Table 1. Entities are sorted by latitude.

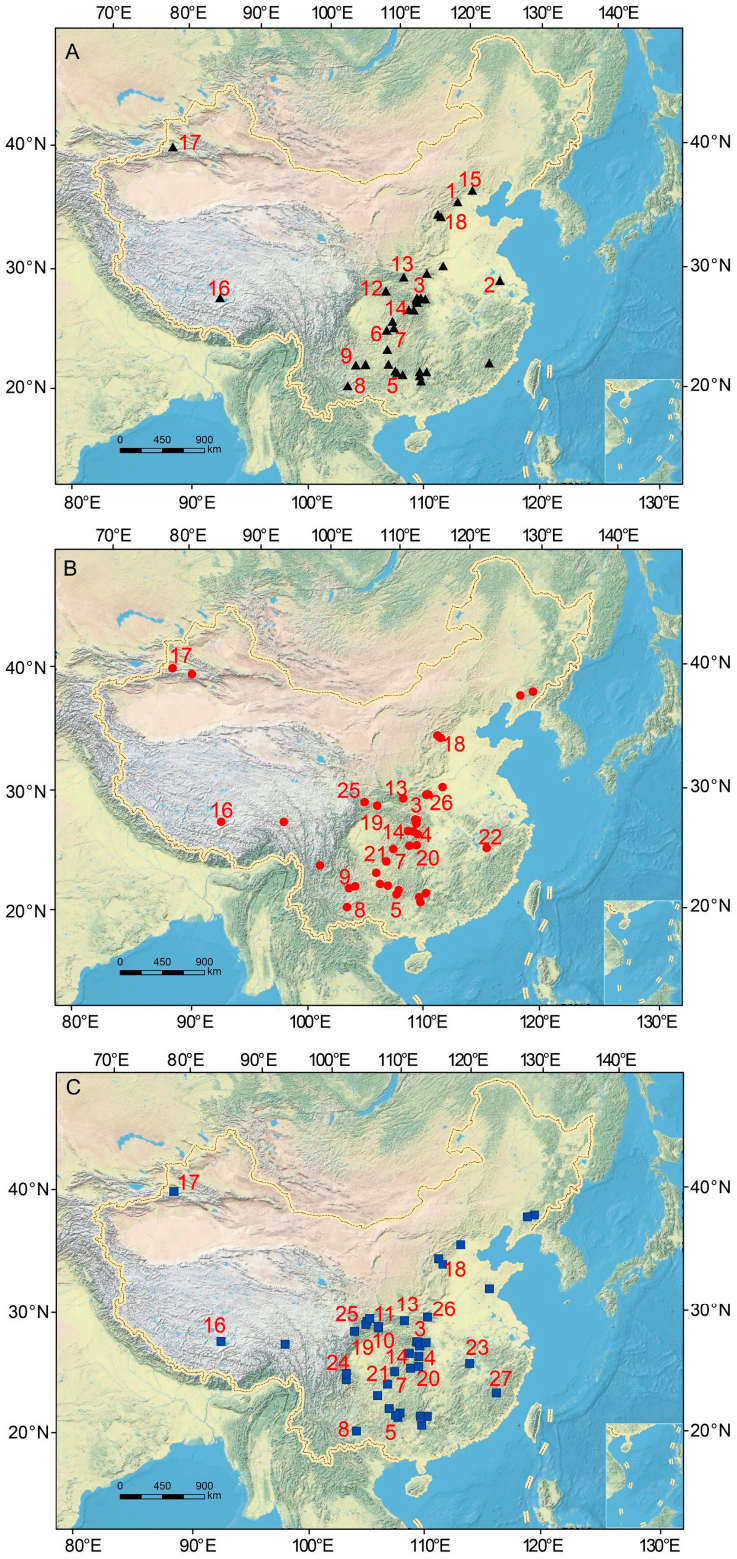

Figure 4. Spatial distribution of speleothem $\delta^{18}O$ records in China during three periods: (**A**) the Late Pleistocene (640 ka–11.7 ka), (**B**) the Holocene (11.7 ka–Present), and (**C**) the last 2000 years. Cave locations numbered 1–17 are the same as in Figure 1. Numbers 18–27 (18: Lianhua (Shanxi); 19: Xianglong; 20: Lianhua (Hunan); 21: Shigao; 22 Shennong; 23: E'mei; 24: Shenqi; 25: Wanxiang; 26: Dongshiya; 27: Yuhua) are records mentioned in the discussion but not in SISAL_v1. Details on each speleothem are given in Table 1.

4. Results and Discussion

4.1. Significance of Speleothem $\delta^{18}O$ as a Climate Proxy in the EASM Area

Chinese speleothem $\delta^{18}O$ records have substantially improved our understanding of the EASM variability on different timescales. However, the paleoclimatic interpretation of Chinese speleothem $\delta^{18}O$ records remains an issue of debate [16,181–193]. For example, there is a strong correlation between speleothem $\delta^{18}O$ series in the EASM and ISM regions, but these data contrast with some other Chinese rainfall records reconstructed by loess and lake sediments [181,182,188]. A few studies suggest that Chinese speleothem $\delta^{18}O$ variability is not controlled by rainfall amount but by moisture source [181,182] or pathway [192], while others conclude that they are not only influenced by the EASM but also to a significant extent by winter temperature [184,185]. Instrumental data and paleoclimatic reconstructions based on other natural archives imply a spatial distribution of rainfall over eastern China that is not consistent with the observations from speleothem $\delta^{18}O$ records. In this regard, Liu et al. [189] argued that speleothem $\delta^{18}O$ records in the region cannot be used as an indicator of EASM intensity. These disagreements partially arose from differing definitions of "ASM intensity". Chinese speleothem $\delta^{18}O$ records, particularly on orbital to millennial scales, reflect first order changes in the fraction of water vapor rained out between tropical sources and cave sites (e.g., [1,12,50]). By this definition, a strong ASM implies a more remote moisture source, with larger rainout along the moisture trajectory, and thus lighter speleothem $\delta^{18}O$ values (e.g., [12]). On orbital scales, this observation is reproducible because Chinese speleothem records follow the NHSI, but their relation to regional rainfall amount remains in dispute [181,182,188,189,193]. Regarding large millennial-scale events, speleothem $\delta^{18}O$ records show consistent positive excursions (i.e., weak EASM) corresponding to cold events that occurred in NH high latitudes. However, the associated spatial changes in rainfall in the EASM domain could have some regional differences, as suggested by model simulations (e.g., [186,194,195]), and as of yet, very limited and difficult to interpret observational data (e.g., [14,196]). The spatial distribution of rainfall in monsoonal China is primarily controlled by changes in the position of the monsoonal rainfall belt in response to changes in EASM intensity coupled with some geographic considerations. It has been suggested that a weak EASM (i.e., consistent positive $\delta^{18}O$ values in the monsoonal China) leads to a southward shift of the rain belt that in turn results in either a dipole (i.e., dry northern China and a wet southern China [44,122,151]) or a tripole pattern (i.e., dry northern and southern China but wet in Central China [14]). Therefore, the speleothem $\delta^{18}O$ records ultimately show the integrated monsoonal signal from the moisture source to the cave sites on orbital to millennial timescales [1], in line with modeling results (e.g., [191,194,197,198]). In this sense, the longstanding disparity between interpretations of Chinese cave $\delta^{18}O$ records may be resolvable through a thorough investigation of site-specific controls on speleothem $\delta^{18}O$ and/or independently corroborating records of rainfall intensity.

The paleoclimatic interpretation and synthesis of speleothem $\delta^{18}O$ records (and their controlling mechanisms) on annual to centennial timescales are further subject to debate, mainly because precipitation $\delta^{18}O$ can be influenced by a broad range of factors (e.g., rainfall amount, moisture source and pathway, storm trajectory, and the seasonality of precipitation). On centennial to decadal timescales, several $\delta^{18}O$ records from the transitional monsoon regions in China show a significant correlation with regional drought/flood indices, suggesting that speleothem $\delta^{18}O$ is controlled by rainfall amount in North China, with lower $\delta^{18}O$ reflecting enhanced precipitation (e.g., [10,44,128,150,151]). On annual to decadal timescales, many modern stalagmite $\delta^{18}O$ records show

significant negative correlations with local instrumental EASM or annual precipitation amount for the last 200 years [44,62,63,128,150,178,199,200]. However, there exists a mismatch between speleothem $\delta^{18}O$ and mean annual rainfall in the south region of the EASM area [54,201]. It has been argued that speleothem $\delta^{18}O$ changes over the EASM region reflect variations in the ratio of water vapor sourced from the ^{18}O-depleted Indian Ocean to the nearby ^{18}O-enriched Western Pacific Ocean—the so-called "circulation effect"—which appears to be controlled by the El Niño-Southern Oscillation (ENSO) cycle [202–204]. Baker et al. (2015) [192] suggested that the atmospheric moisture pathway might significantly influence precipitation and speleothem $\delta^{18}O$ in the monsoonal China. In SE China, especially in the region of "spring persistent rain", speleothem $\delta^{18}O$ variability seems to be controlled primarily by the seasonality of rainfall (i.e., the ratio of EASM precipitation versus that from the remaining seasons), which is modulated by ENSO on annual to decadal timescales [54,205]. Furthermore, the "circulation effect" may play an important role in Central China, where the ISM and the EASM dominate alternatively on annual to multidecadal scales, depending on the position/strength of the Western Pacific Subtropical High (WPSH) [50]. Some speleothem $\delta^{18}O$ records also show close links with the Pacific Decadal Oscillation (PDO) [54,128,199], WPSH [50,54], and ENSO [54,201]. A range of climate dynamics thus modify speleothem $\delta^{18}O$ values on annual to centennial scales, further complicating the assessment of its relationship with EASM variability. Nevertheless, it can be generalized that when the ENSO is in the cold mode (i.e., La Niña), the WPSH intensifies and/or shifts westward, whereas during the cold mode of the PDO, the EASM tends to transport more moisture from more distal regions into northern regions in China, resulting in lighter speleothem $\delta^{18}O$ values and vice versa [54,203,205].

In summary, Chinese speleothem $\delta^{18}O$ records seem to be inversely related to EASM intensity in orbital to millennial timescales. Thus, we interpret low and high values of Chinese speleothem $\delta^{18}O$ records on these timescales to reflect a "strong" and a "weak" monsoon, respectively. This is broadly consistent with both theoretical and empirical studies (e.g., [1,2,5,8,9,14,191,194,196–198]. The interpretation of Chinese speleothem $\delta^{18}O$ records on annual to centennial timescales is more complex. At these short time-scales, the speleothem signal is understood to reflect summer rainfall, the location of the moisture source and storm trajectory, or the seasonality of precipitation as associated with changes in ocean–atmosphere circulations. More empirical and theoretical studies remain critical in order to further understand Chinese speleothem $\delta^{18}O$ records.

4.2. Late Pleistocene Variations of the ASM and Westerly Climates Recorded by Speleothem $\delta^{18}O$ Records

4.2.1. Orbital-Scale Changes

Seven published speleothem $\delta^{18}O$ records in China have long temporal coverage for the orbital-scale ASM and westerly climate variations (Figures 3a and 4a), for example, the records from Hulu [5], Dongge [12], Sanbao [1,9], Xiaobailong [13], Kesang [21], Yangkou [166], and Yongxing [173] caves. All these records, except Yongxing, are in SISAL_v1.

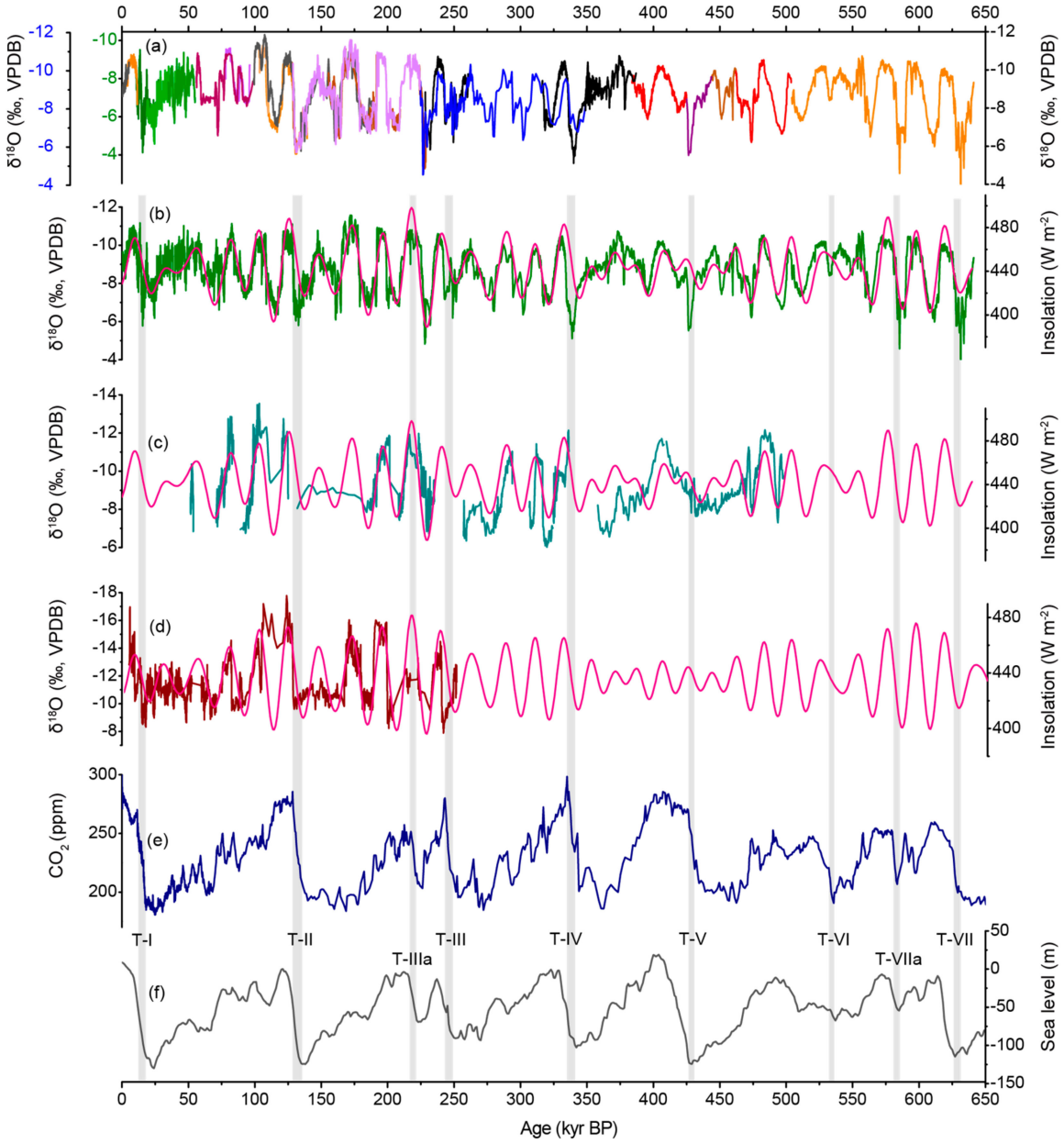

Figure 5. Orbital scale changes in speleothem $\delta^{18}O$ records from China and comparison with other records. (**A**) Multi-speleothem record from China: three records from the Hulu Cave (green curves; green left *y*-axis), two records from the Linzhu Cave (blue curves; blue left *y*-axis), and 16 records from the Sanbao Cave (all other colors; black right *y*-axis). (**B**) The 640 kyr EASM composite record from (**A**) [1]. (**C**) The composite $\delta^{18}O$ record from the Kesang Cave (cyan curve) [21]. (**D**) The composite $\delta^{18}O$ record from the Xiaobailong Cave (brown curve) [13]. Pink curves in panels **B**–**D** show 21 July insolation at 65 °N [206]. (**E**) The composite CO_2 record [207]. (**F**) The composite sea level record [208]. Vertical gray bars mark the timing of seven glacial terminations, which correspond with weak monsoon intervals.

The composite stalagmite $\delta^{18}O$ record from the Hulu [5], Sanbao [9], and Linzhu caves [1,9] (Figure 5a) is dominated by the 23 kyr precessional cycles that are in phase with NHSI (21 July, 65 °N) (Figure 5b) [1]. On the basis of this composite, Cheng et al. [1] demonstrated that glacial terminations are separated by either four or five precession cycles, supporting the idea that the "100 kyr" ice-age cycle is an average of discrete numbers of precession cycles [209]. The timings of the past six glacial terminations precisely coincide with the timing and sequence of the termination events [1] (gray bars in

Figure 5) as established from ice cores (Figure 5e) and marine sediments (Figure 5f). Changes in NHSI caused by the Earth's precession appear to be the main driver of the last seven ice-age terminations, as well as of the millennia-long intervals of reduced monsoon intensity associated with each of the terminations [1]. These observations are consistent with a classic NHSI trigger: an initial retreat of the northern ice sheets releases meltwater and icebergs into the North Atlantic Ocean, altering oceanic and atmospheric circulation patterns and associated heat and carbon fluxes, which causes an increase in atmospheric CO_2 (Figure 5e) and Antarctic temperatures and finally drives the termination in the Southern Hemisphere [11]. Increasing CO_2 and summer insolation further amplifies the recession of northern ice sheets, accelerating a rise in sea level and CO_2 through a positive feedback cycle [11] (Figure 5).

Kesang Cave is located in the eastern side of Central Asia, currently a semiarid–arid region dominated by the westerly climate (Figure 1). High-resolution (~200 year) and high-precision $\delta^{18}O$ records from Kesang Cave cover most of the last 500 kyr [21] (Figure 5c). This record shows that climate change in this region exhibits a precessional rhythm with abrupt inceptions of low $\delta^{18}O$ at times of high NHSI, followed by gradual $\delta^{18}O$ increases that track the decline in insolation. While it is unclear whether the Kesang record suggests a possible incursion of the ASM rainfall or related moisture into the Kesang site and/or adjacent areas during the high NHSI times, it shows that orbital changes in the westerly hydro-climate are in phase with ASM variations (Figure 5b,c), which is supported by model simulations [34,197,210].

A speleothem $\delta^{18}O$ record from Xiaobailong Cave in SW China characterizes changes in the ISM over the last 252 kyrs [13] (Figure 5d). This record is dominated by 23 kyr precessional cycles (Figure 5d) and, to some extent, exhibits glacial–interglacial changes (Figure 2 in Cat et al. (2015) [13]) that are in agreement with marine and other terrestrial proxies, but contrast with other speleothem $\delta^{18}O$ records from eastern China [13]. It has been corroborated by isotope-enabled global circulation modeling that the different responses of South and East Asian speleothem $\delta^{18}O$ records (Figure 5) might be caused by the exposure of the land bridge in the western equatorial Pacific during glacial periods, which results in more depleted precipitation/stalagmite $\delta^{18}O$ over eastern China [13]. However, it remains an open question whether the observed glacial–interglacial variations are a manifestation of the large amplitude of ISM variations on the orbital-scale. Indeed, the ISM amplitude observed in Xiaobailong $\delta^{18}O$ records at this temporal scale is ~7–8‰ [13], which is much larger than the typical EASM amplitude (~3–4‰, [1]). Absolute speleothem $\delta^{18}O$ values reflecting ISM precipitation are also lower (Figure 5b,d, Figure 2 in Reference [13]). In addition, similar ranges in modern precipitation $\delta^{18}O$ and glacial–interglacial speleothem $\delta^{18}O$ values have been observed between SW and SE China [211]. A possible explanation might involve differences in moisture sources and trajectories in the ISM and EASM regimes. While, the ISM moisture is mainly derived from the remote Indian Ocean, the source of EASM moisture is apparently more complex, with moisture originating from the nearby Pacific Ocean, the South China Sea, and/or the Bay of Bengal (Figure 2) [203,212]. This may partially explain the low $\delta^{18}O$ values observed in speleothems and precipitation in SW China compared to SE China.

Overall, EASM speleothem $\delta^{18}O$ records (e.g., Sanbao and Hulu [1]) show a temporal variability that is coherent with ISM records (e.g., Xiaobailong [13] and Bittoo [213]) on both orbital and millennial timescales, indicating similar forcing factors. For example, the EASM and ISM exhibit a coupled response to changes in NHSI without significant temporal lags [213]. Additionally, two speleothem $\delta^{18}O$ records from the Dongge [12] and Yangkou [166] caves in Guizhou and Chongqing (SW China), where the relative impact of EASM/ISM cannot be disentangled, track changes in NHSI on orbital timescales. As such, we suggest that on orbital timescales, speleothem records from both EASM and ISM regions are dominated by the Earth's precessional cycle that is in phase with NHSI. This coherence supports the idea that tropical/subtropical monsoons predominantly and directly respond to changes in NHSI [213].

4.2.2. Millennial-Scale Climate Events

A large number of Chinese speleothem $\delta^{18}O$ records can be utilized to characterize millennial-scale climate variability corresponding to Dansgaard–Oeschger events [214] and Heinrich stadials/interstadials [215] in the Northern Hemisphere. This list include records from the Hulu [5,9,71], Sanbao [9], Dongge [12], Dragon [52], Songjia [139], Suozi [216], Xinya [163], Xinglong [161], Kulishu [77,161], Wulu [43,146], Kesang [21], Xiaobailong [13,160], Dashibao [43], Yangkou [167–169], Sanxing [119], Yongxing [173], Qingtian [69], Xianyun [158,159] caves, etc. Among the above records, the Hulu [5,9,71], Sanbao [9], Kesang [21], Dongge [12], Xinya [163], Yangkou [167–169], Kulishu [77], Xinglong [161], Xiaobailong [160] and Suozi [216] records are incorporated in the SISAL_v1 database.

Millennial-scale events during the last glacial were reconstructed using three stalagmites from the Hulu Cave [5]. The Hulu record shows that the EASM intensity changed in agreement with Greenland's temperature between 75 and 11 kyr BP (Figure 6a,b), indicating a close link between the EASM and North Atlantic climate. Recently, the Hulu record has been significantly improved in terms of both sample resolution and dating (Figure 6b) [64]. A close comparison between the Sanbao, Hulu, and Greenland ice core records suggests that the monsoonal interstadials between the last and penultimate glacial periods are similar in their duration and frequency, implying that the millennial fluctuations may be synchronous under glacial conditions [9].

The millennial weak EASM events are generally considered to be caused by the decay of the northern ice sheets, resulting in the flux of ice and meltwater into the North Atlantic. The ensuing slowdown in Atlantic Meridional Overturning Circulation (AMOC) generated a cold anomaly over the North Atlantic, resulting in reorganizations of oceanic and atmospheric circulations, and, in turn, the weak monsoon events [1,5]. By removing orbital-scale components from the 640 kyr composite speleothem $\delta^{18}O$ record and the Antarctic δD record (Figure 3 in Reference [1]), we obtained the residual $\Delta\delta^{18}O$ and $\Delta\delta D$ records, respectively [1]. The $\Delta\delta^{18}O$ and $\Delta\delta D$ records are remarkably similar and negatively correlated [1]. A high-resolution reconstruction of EASM variability between 88 and 22 kyr BP from the Yongxing Cave in central China ([173]; Figure 6c) is strikingly similar to the Hulu records, suggesting a regionally coherent pattern of speleothem $\delta^{18}O$ on millennial timescales (Figure 6b,c). After removing the 65 °N insolation signal from the Yongxing $\delta^{18}O$ record, the residual $\Delta\delta^{18}O$ was also strongly anti-phased with Antarctic temperature variability on sub-orbital timescales during the Marine Isotope Stage (MIS) 3 (Figure 2 in Reference [173]). It seems evident that during North Atlantic Heinrich events, Antarctica became warmer and the ASM weakened (Figure 6). These results provide a robust linkage between northern and southern high-latitude and low-latitude monsoon climates that likely operated via the bi-polar seesaw mechanism [217,218]. The strong coupling between EASM circulation and millennial-scale climate at high latitudes indicates that atmospheric circulation changes are important in transmitting abrupt climate signals globally. On the other hand, the more gradual changes observed in the EASM and in Antarctica compared to Greenland's temperature during Heinrich events (Figure 6) implies that oceanic circulation and/or sea surface temperatures (SSTs) also play an important role in the propagation of the climatic signal on millennial–centennial scales.

The Xiaobailong $\delta^{18}O$ record (Figure 6d) reveals that the millennial variability of the ISM was synchronous with the EASM, as recorded by the Hulu and Yongxing records (Figure 6b,c), but with systematically lower $\delta^{18}O$ values. In addition, some ISM millennial-scale features (Figure 6d) seem to resemble the temperature changes recorded in the Antarctic ice core records (Figure 6f), particularly during the Heinrich events, consistent with the mechanism previously described. However, a number of authors have emphasized the potential role of Antarctic glacial and sea-ice retreat to influence the ISM region through perturbations to oceanic overturning circulation that originated with freshwater discharge from the southern ice sheets (e.g., [1,2,58,160,169,173]).

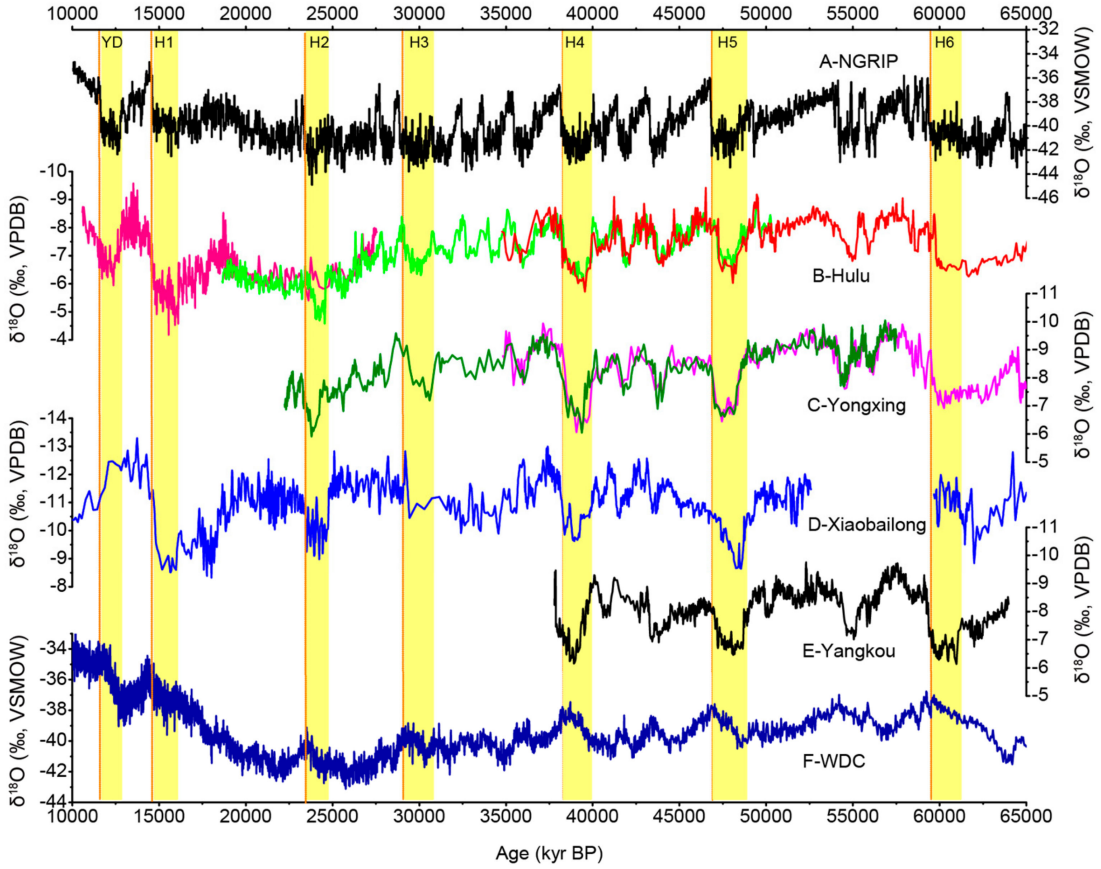

Figure 6. Comparison of Chinese speleothem $\delta^{18}O$ records with bi-polar ice core $\delta^{18}O$ records between 65 and 10 kyr BP. (**A**) NGRIP $\delta^{18}O$ record [219]; (**B**) Hulu Cave (H82 in pink; MSD in green; MSL in red); (**C**) Yongxing Cave (YX51 in green; YX55 in pink; YX46 in purple); (**D**) Xiaobailong Cave; (**E**) Yangkou Cave; (**F**) WDC $\delta^{18}O$ record from the Antarctic [220]. Yellow bars indicate Younger Dryas (YD) and Heinrich events (H1–H6) which occurred in the North Atlantic [215].

Some differences between the EASM and ISM are also notable, for example, in the Shizi $\delta^{18}O$ record, which exhibits a significant negative excursion around 47.5–46.6 kyr BP that was not clearly documented in the other two $\delta^{18}O$ records from SW China [132]. The Sanxing $\delta^{18}O$ record shows a weakening ISM trend from 22 to 17 kyr BP, while the Hulu and Qingtian records express a 3 kyr period with an intensified EASM event during that period [120]. The decoupling of the EASM and ISM may be due to the different sensitivities of the two ASM sub-systems in response to internal feedback mechanisms associated with the complex geographical or land–ocean configuration, as well as SST differences between the Indian and Pacific oceans [75,120].

A large number of Chinese speleothem records cover the Younger Dryas (YD) and Bølling–Allerød (BA) events during the last deglaciation, including samples from the Hulu [5], Dongge [12,45], Yamen [165], Songjia [139], Qingtian [99,100], Kulishu [77], Haozhuzi [14,58], Longfugong [85], Xianglong [152], Linyi [83], and Lianhua [82] caves. The timing, structure, and mechanism of the YD event have been discussed in detail in the context of the Hulu, Dongge, Yamen, Qingtian, and Kulishu cave records. These $\delta^{18}O$ time series are fixed by precise chronologies and, therefore, provide detailed information on the structure of the YD cooling, which is interpreted in Asia as a weakened monsoon event. Based on the Hulu records, the BA event lasted from 14,645 ± 60 to 12,823 ± 60 yr BP and the YD event lasted from 12,823 ± 60 to 11,473 ± 100 yr BP [5]. The Dongge record shows striking similarity with the Hulu record during both periods despite the fact that ~1200 km separates the caves [12]. A record from Yamen Cave indicates that the onset and termination of the YD monsoon event are 12,850 ± 50 and 11,500 ± 40 yr BP, respectively [165]. The QT $\delta^{18}O$ record from Qingtian Cave [99],

which is based on annual-layer counting and ^{230}Th dates, documents with ultra-high precision the transition into the YD. A new δ^{18}O record (QT16) from the same cave reveals a gradual shift into the YD from 12,970 ± 30 to 12,290 ± 80 yr BP and a rapid termination of YD within ~11 yrs [100]. Based on annual-layer counting, the record from Kulishu Cave [77] indicates that the shift into the YD began at 12,850 ± 40 yr BP and lasted for ~340 yr, while the end of the event began at 11,560 ± 40 yr BP as an abrupt positive δ^{18}O shift that lasted less than 38 yrs (or a best estimate of ~20 yrs). These results are broadly similar to other speleothem records from Hulu, Dongge, Yamen, and Qingtian Caves. During the mid-YD, three centennial wetting peaks in the Qingtian record, consistent with those in the Kulishu record, show similar structures to Greenland's temperature variations (i.e., three warming peaks) [77,100].

The weak EASM during the YD event may be tied to a weakened AMOC, which affects North Atlantic climate and, in turn, the mean latitudinal position of the ITCZ, resulting in a decrease in northern low-latitude precipitation [5,77,100]. Cross-spectral analysis of the NGRIP and QT16 records shows a coherent power of ~200 yr that is prominent during the YD event, partly supporting the hypothesis that centennial variability in mid-YD is associated with solar activity [100]. The consistent age control of this ASM YD structure indicates that the ASM region experienced a longer transition into the YD than the corresponding Greenland temperature shift by at least 130 yr [221], implying that, apart from the direct link between Greenland and the ASM via atmospheric circulation, oceanic circulation changes may have been important. Recently published trace-element ratios (Sr/Ca, Mg/Ca, Ba/Ca) and δ^{13}C data from the Haozhuzi Cave in the middle Yangtze region indicate a wetter central eastern China during the last deglaciation, when the North Atlantic was in the cold episodes (the Heinrich 1 and YD events), even though the speleothem δ^{18}O record suggests a weaker monsoon state [14]. In accordance with the "jet transition hypothesis" [34], some studies suggest that a cold North Atlantic climate leads to a southward shift of the ITCZ, which, in turn, results in a lengthening of the mei-yu rains and a shortening post-mei-yu stage [14].

4.3. Stalagmite δ^{18}O Records During the Holocene

A large number of speleothem records have been published, which document the Holocene climate in China (Figures 3b and 4b); however, only some of these records are in the SISAL_v1 database: i.e., C996-1 and C996-2 from Jiuxian Cave [75], TM18a and TM18b from Tianmen Cave [25], XBL29 and XBL48 from Xiaobailong Cave [13], KS06-A-H, KS08-1-H, and KS08-2-H from Kesang Cave [21], SB10, SB26, SB27, SB43, SB44, and SB49 from Sanbao Cave [113], HS4 from Heshang Cave [15], D4 from Dongge Cave [45], and ZLP1 and ZLP2 from Zhuliuping Cave [179]. Although with little metadata, δ^{18}O time-series for other Holocene records are available at the National Centers for Environmental Information (NCEI): CNKS-2, CNKS-3, CNKS-7, and CNKS-9 from Kesang Cave [22]; LH4, LH5, and LH9 from Lianhua Cave (Shanxi Province) [82]; XL2, XL16, and XL26 from Xianglong Cave [151]; A1 [222] and LHD5 [81] from Lianhua Cave (Hunan Province); and DA [8], D4 [45], and DAS [47] from Dongge Cave. The data from some additional published Holocene records are not publicly available, precluding their incorporation in this review: Xiangshui Cave [49,153], Dongge Cave [47], Nuanhe and Water Caves [223], Wanxiang Cave [27], Baigu Cave [41], Shigao Cave [125], Dark Cave [42], Magou Cave [86], Niu Cave [88], and Bengle Cave [26]. In this section, we used the most relevant Holocene records (from SISAL_v1 and other public repositories as indicated in Table 1) to discuss the long-term dynamic changes of ASM intensity and the interaction between the EASM and ISM during the Holocene on millennial to centennial timescales.

4.3.1. Holocene δ^{18}O Records Forced by Insolation

A progressive long-term increase in δ^{18}O values was observed in the records from Lianhua (Shanxi Province) [82], Jiuxian [75], Xianglong [151], Sanbao [113], Heshang [15], Lianhua (Hunan Province) [81,222], Dongge [8,45,47], Shigao [125], and Tianmen [25] caves, following the decreasing trend of NHSI (Figure 7a–j). The same trend was shown in records from Xiangshui [49,153], Nuanhe

and Water [223], Wanxiang [27], Baigu [41], Dark [42], Niu [88], Zhuliuping [179], Magou [86], and Xiaobailong [13] caves, further confirming that changes in ASM intensity are primarily controlled by NHSI on orbital timescales. A synthesized Holocene record based on 16 stalagmites from the monsoonal China (Figure 7k) clearly tracks changes in NHSI [224], in agreement with other EASM records and confirming that $\delta^{18}O$ records are a valid proxy for ASM intensity [224].

Climate dynamic factors influencing Holocene speleothem $\delta^{18}O$ changes in Kesang [21,22] and Baluk [23] caves in NW China are more complex. A synthesis of speleothem $\delta^{18}O$ records from Central Asia (Uzbekistan to western China) reflects a supra-regional pattern of climate variability on orbital to millennial timescales [196], but local hydroclimatic changes during the Holocene are not in phase with the orbitally paced, regional signal of the Asian monsoons. For example, carbon-isotope and trace-element proxies of hydroclimate are shown to lag the supra-regional climate variability by up to several thousand years. Cai et al. (2017) [22] proposed that both moisture source and the amount of precipitation contributed to $\delta^{18}O$ variability in the Kesang Cave during the early and middle Holocene. On the other hand, the Baluk $\delta^{18}O$ record strongly suggests a link between hydroclimatic variability in northwestern China and solar activity on centennial-to-multi-decadal timescales [23]. In the following discussion, we focused on the Holocene records from the monsoonal China.

4.3.2. Spatio-Temporal Distribution of $\delta^{18}O$ Records During the Holocene

In the lower-latitude monsoonal region, the increasing $\delta^{18}O$ trend observed (waning of the Holocene Climatic Optimum; hereafter HCO) commenced as early as ~7.5 kyr BP, while at higher latitudes this excursion started progressively later: ~7.0 kyr BP in the Dongge record, ~5.3 kyr BP in the Heshang record, ~4.7 kyr BP in the Sanbao record and ~4.5 kyr BP in the Jiuxian record [75]. This meridional pattern of HCO waning suggests an asynchronous change in EASM intensity during the Holocene, which could be explained by the response of a coupled tropical and subtropical monsoon system to changes in insolation gradients and, in turn, variable thermal forcing associated with the regional geographical configuration [75]. SST variability in western tropical Pacific may also have an important influence on EASM variability in central and northern China via its impact on WPSH, which regulates monsoon front migration. Higher SST in the western tropical Pacific can force a northward migration of the subtropical high over East Asia, which implies a northward shift of the monsoonal front and associated rain band. This hypothesis was reinforced by a new Holocene record from Shigao Cave, SW China [125], that shows an increasing trend starting at ~6 kyr BP and that is in agreement with the spatial pattern proposed by Cai et al. (2010) [75]. Some studies also suggested that the spatially asynchronous ending of the HCO in Asia may be attributed to SST changes in the western tropical Pacific [75,125], which is an important moisture source region of the East Asian monsoon.

To estimate the timing and duration of the HCO in Chinese stalagmite $\delta^{18}O$ records, we analyzed 10 Holocene records using RAMPFIT [225]: Lianhua (Shanxi) [82], Jiuxian [75], Xianglong [151], Sanbao [113], Heshang [15], Lianhua (Hunan) [81], Dongge [8,45], Shigao [125], and Tianmen [25] cave records. RAMPFIT is a weighted-square method commonly used to determine a ramp between different states of a variable in a time series [225]. Our results show that the HCO, as identified by low $\delta^{18}O$ values, is spatially synchronous from South to North China (Figure 7). This disagreement with previous findings is partially attributable to dating uncertainties and different $\delta^{18}O$ temporal resolutions. However, the actual spatio-temporal pattern and underlying mechanism may be more complex than has previously been recognized [75]. The results presented here call for more high-quality Holocene records to reconcile these contradicting observations and to gain insights into the processes controlling the HCO signature in SE Asia.

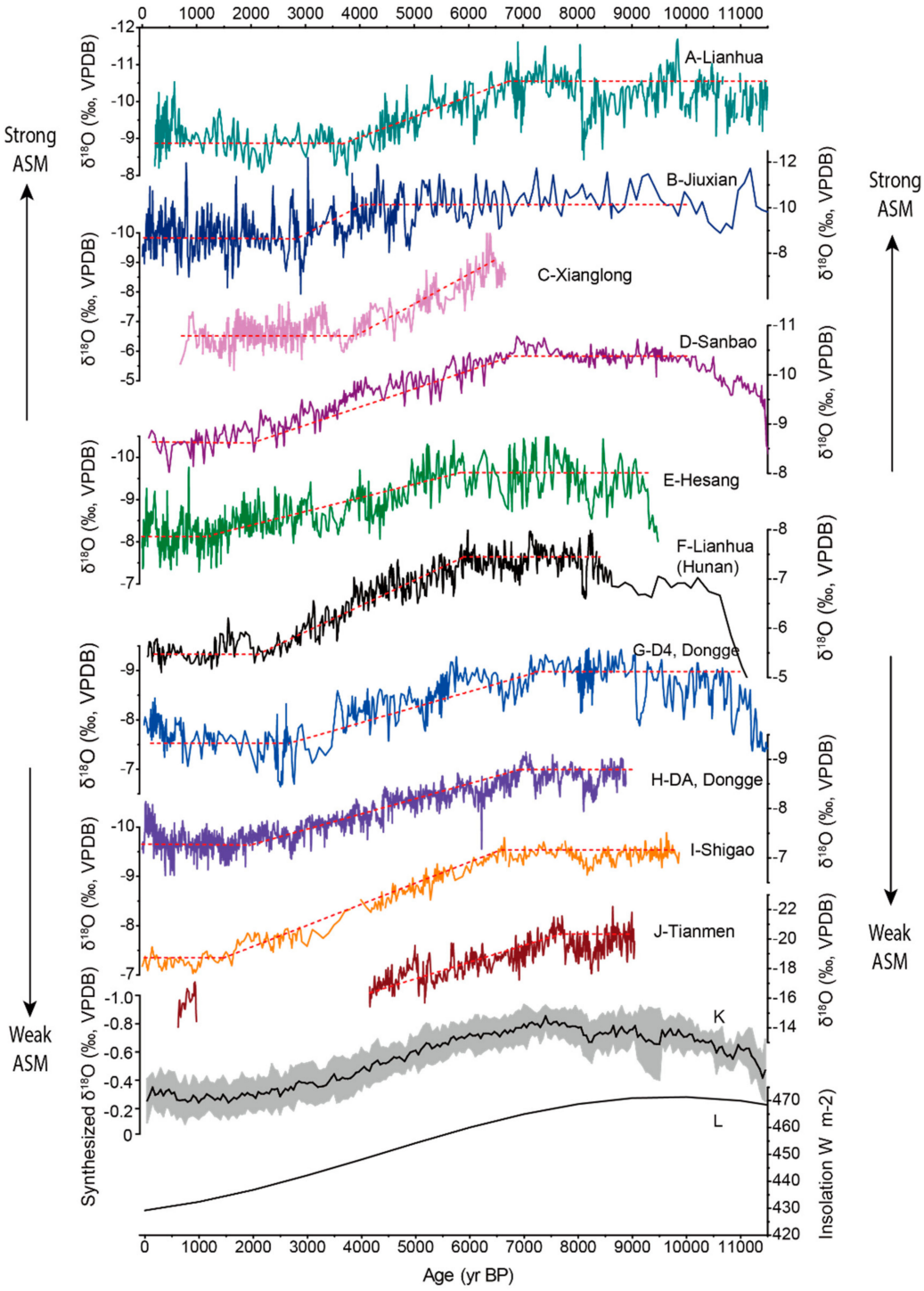

Figure 7. Holocene stalagmite $\delta^{18}O$ records from China. (**A**) Composite record from Lianhua Cave (Shanxi) [74]; (**B**) Composite record (C996-1 and C996-2) from Jiuxian Cave [75]; (**C**) Composite record (XL2, XL16 and XL26) from Xianglong Cave [151]; (**D**) Composite record (SB27 and SB43) from Sanbao Cave [113]; (**E**) HS4 record from Heshang Cave [15]; (**F**) LH2 record from Lianhua Cave [81]; (**G**) D4 record from Dongge Cave [45]; (**H**) DA record from Dongge Cave [8]; (**I**) Composite record (SG1 and SG2) from Shigao Cave [125]; (**J**) Composite record (TM18a and TM18b) from Tianmen Cave [25]; (**K**) Synthesized speleothem $\delta^{18}O$ record calculated averaging 16 records in the monsoonal China [224], gray shadow indicates standard deviations; (**L**) 21 July insolation at 65 °N [206]. The red, dashed lines in (**A**–**J**) show the best fit using the RAMPFIT program [225].

4.3.3. Millennial-Scale Events During the Holocene

At millennial timescales, the $\delta^{18}O$ time series from Dongge is punctuated by eight weak monsoon events each lasting ~1 to 5 centuries [8]. Significant multi-centennial variability is also evident in the Heshang record, with notably dry periods during the 8.2 kyr BP event and at 4.8–4.1 kyr BP, 3.7–3.1 kyr BP, 1.4–1.0 kyr BP and the Little Ice Age (LIA) [15]. These weak EASM events are causally linked to North Atlantic ice-rafting debris (IRD) events or Bond events through southward displacement of westerly and ITCZ circulation, in particular, the 8.2 kyr [61,226] and 4.2 kyr [122] events. The 4.2 kyr event in the EASM region may have contributed to the collapses of the Chinese Neolithic culture [227]. An antiphase pattern was observed between the EASM and the South American summer monsoon (SASM) during the 8.2 kyr event [228], highlighting the global extent of this event. The teleconnection is explained by a slowdown in AMOC (triggered by a glacial lake draining event) that led to a cooling of the North Atlantic climate and a southward migration of the ITCZ, in turn reducing EASM and increasing SASM intensities [8,61,226,228].

During the 4.2 kyr BP event, wet conditions are reconstructed from sites in central and southern China (Xianglong, Jiuxian, Sanbao and Heshang $\delta^{18}O$ records), while dry conditions are reconstructed from one site in northern China (Lianhua (Shanxi) $\delta^{18}O$ record) (Figure 8) [151]. A new high-resolution (6~30-year) $\delta^{18}O$ record from Shennong Cave (Figure 8f) in SE China provides a critical evidence supporting the similar "north dry, south wet" pattern during the 4.2 kyr event [122]. The Dongge and Mawmluh $\delta^{18}O$ records also suggest a dry hydro-climate in SW China and the ISM region, respectively (Figure 8g,h). Thus, it appears that during this event, the monsoonal rain belt may have stayed longer in the south, and shorter in the north [122,151]. These weakened EASM and ISM may have been triggered by the reduced AMOC as a result of the melting icebergs in the North Atlantic (Figure 8i) [122,151]. However, a recent paleoclimate data synthesis with climate-model support for western Eurasia proposed that expansion of the Siberian High is a more plausible explanation for the geographic distribution of climate perturbations near 4.2 kyr BP [229].

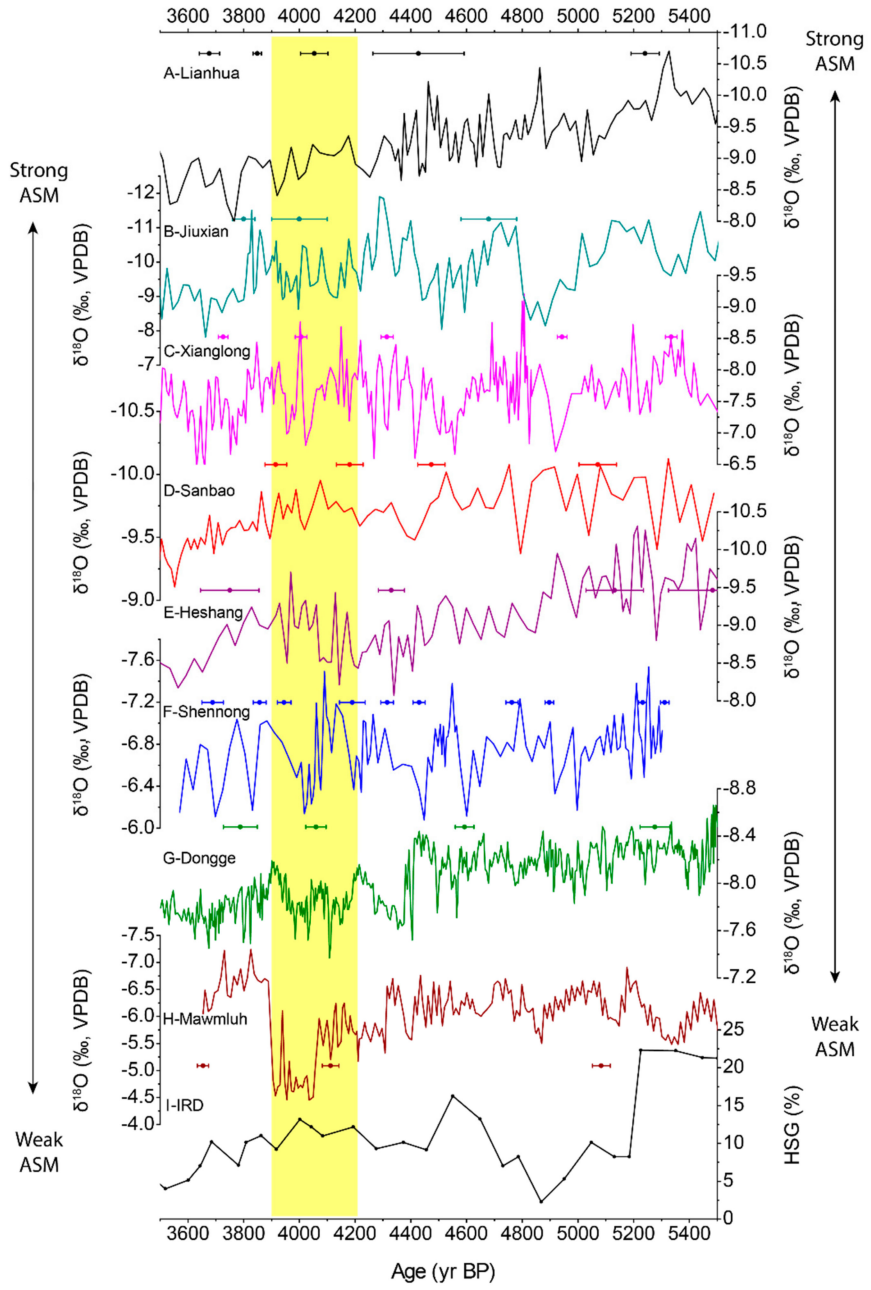

Figure 8. Speleothem $\delta^{18}O$ records for the period 5500–3500 yr BP. (**A**) Lianhua Cave (Shanxi) [82]; (**B**) Jiuxian Cave [75]; (**C**) Xianglong Cave [151]; (**D**) Sanbao Cave [113]; (**E**) Heshang Cave [15]; (**F**) Shennong Cave [122]; (**G**) Dongge Cave [8]; (**H**) Mawmluh Cave [230] and (**I**) the ice-rafted hematite-stained grains (HSG) record from the North Atlantic [231]. ^{230}Th dates and error bars are shown at the top of each speleothem $\delta^{18}O$ time-series. The yellow bar marks the interval 4.2-3.9 kyr BP, when drier than average conditions are reconstructed in northern and SW China and wet conditions are found in central and SE China.

4.4. Climate Variability During the Last 2000 Years

There are at least 15 published speleothem $\delta^{18}O$ records that fully or partially cover the last 2000 years (Figures 3b and 4c, see Table 1 for details). Unfortunately, the records from Longquan [232], Xiniu [162], Buddha [233], Qingtian [234] and Qixing [109] caves are published in Chinese journals and their data have not been made publicly available. The following discussion will focus on the three Chinese speleothem $\delta^{18}O$ records in SISAL_v1 as well as the records available from Table 1: WX42B

from Wanxiang Cave [10], HY-1, HY-2 and HY-3 from Huangye Cave [63], DA from Dongge Cave [8], HS4 from Heshang Cave [15] and SQ1 from Shenqi Cave [235].

Strong links between the EASM and the NH temperature [236], the temperature of the warm season in northern China [127] and solar variability [237,238] have been suggested from Huangye and Wanxiang $\delta^{18}O$ records [10,63] (Figure 9). However, such a strong link is unclear in Shenqi, Jiuxian, Sanbao, Dongge and Heshang records (Figure 9g–k). A comparison of speleothem $\delta^{18}O$ from Dayu, Dongge, Wanxiang, Buddha, Heshang and Lianhua caves in the EASM region over the last 750 years revealed a large variability of monsoon precipitation on decadal to centennial scales with spatial differences between southern and northern regions, likely due to changes in rain belt dynamics that ultimately relate to variations in ASM intensity [44,235].

The Medieval Climate Anomaly (MCA, 950–1250 CE) and the LIA (1400–1700 CE) [239] also manifest as $\delta^{18}O$ anomalies in Chinese cave records. A warm Northern Hemisphere MCA could drive the ITCZ northward thereby intensifying the EASM. This situation is consistent with observations of increased precipitation in northern China (Wanxiang and Huangye $\delta^{18}O$ records) and SW China (Shenqi $\delta^{18}O$ record) but decreased precipitation in southern China (Dongge and Heshang $\delta^{18}O$ records) (Figure 9). In contrast, cold conditions in the Northern Hemisphere during the LIA drive the ITCZ southward, thereby weakening the EASM. This results in drier conditions in northern China (Wanxiang and Huangye $\delta^{18}O$ records) and wetter conditions in southern China (Dongge and Heshang $\delta^{18}O$ records), respectively (Figure 9). In general, precipitation in the EASM region shows a "north wet/south dry" pattern during the MCA and a "north dry/south wet" pattern during the LIA [235], similar to earlier Holocene events. Studies of Chinese speleothem records also provide unique and robust tests of the relationships between speleothem $\delta^{18}O$, the occurrence of droughts, and societal unrest [27,28,150]. Besides the influence of Northern Hemisphere, some studies suggest that variations in low-latitude monsoon precipitation are significantly influenced by shifts in the mean position of the ITCZ and WPSH, which is further mediated by solar activity [235] and tropical SSTs [46,47]. A number of studies suggest that a decreased gradient in the tropical Pacific SST and the associated cold phase of ENSO (La Niña phase) would result in a northeastward extension of the Western Pacific Subtropical High (WPSH), which would lead to more moisture being taken up from the remote Indian Ocean compared to the Pacific [203,204,240]. This signal would be captured by negative excursions in the speleothem $\delta^{18}O$ records, as seen in Wanxiang, Huangye and Shenqi $\delta^{18}O$ records. A more La Niña-like phase in the tropical Pacific during the MCA and more El Niño-like phase during the LIA have been noticed as major driving factors [193,239] that impose profound influences on the EASM system. However, the opposite mechanism linking the dominant El Niño-like and La Niña-like conditions to the MCA and LIA, respectively, has also been proposed [241]. The phase status of ENSO during both the MCA and LIA remain a debate issue [193], and further studies are clearly needed.

On a decadal scale, the Pacific Decadal Oscillation (PDO) and the ENSO are strongly correlated, with positive PDO indices (warm PDO phase) corresponding to El Niño events (warm ENSO phases) [54]. During the cold phases of PDO and ENSO (La Niña phase), the WPSH weakens and/or shifts eastward, resulting in a tendency by the EASM system to transport moisture from more distal regions into northern China—as reflected by a lower $\delta^{18}O$ in precipitation [54,203]. This pattern is consistent with the observed positive correlation between spelethem $\delta^{18}O$ from Wanxiang [10], Huangye [63], Shihua [128], E'mei [54] and the normalized multi-speleothem $\delta^{18}O$ composite from monsoonal China and the PDO index on decadal scales (Figure 10), which suggests that speleothem $\delta^{18}O$ is modulated by large-scale atmospheric-ocean circulation patterns.

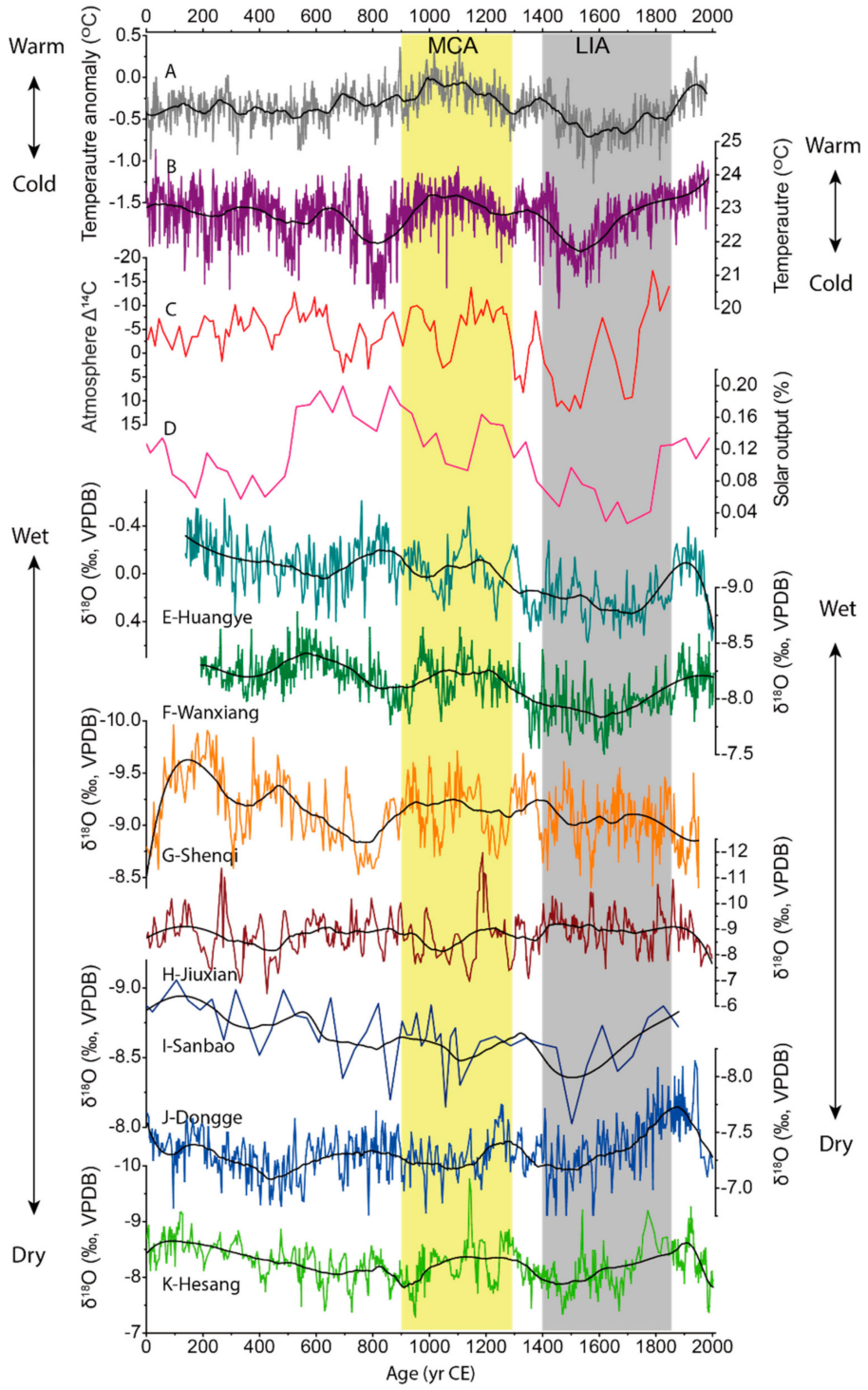

Figure 9. Chinese speleothem $\delta^{18}O$, solar activity and temperature curves for the last 2000 yrs. (**A**) Temperature anomaly for the Northern Hemisphere [236]; (**B**) Warm season temperature in northern China from Shihua Cave [127,225]; (**C**) Atmospheric $\Delta^{14}C$ [237]; (**D**) Solar output [238]; (**E**–**K**) Speleothem $\delta^{18}O$ records from Huangye [63], Wanxiang [10], Shenqi [235], Jiuxian [75], Sanbao [113], Dongge [8] and Heshang caves [15]. The black, solid line in panels A and B is the 100-year running mean. Black lines in panels C–K is the 50-year running mean. Yellow and gray bars show the intervals best defining the Medieval Climate Anomaly (MCA) and Little Ice age (LIA) based on the Northern Hemispheric temperature anomaly (**A**), respectively.

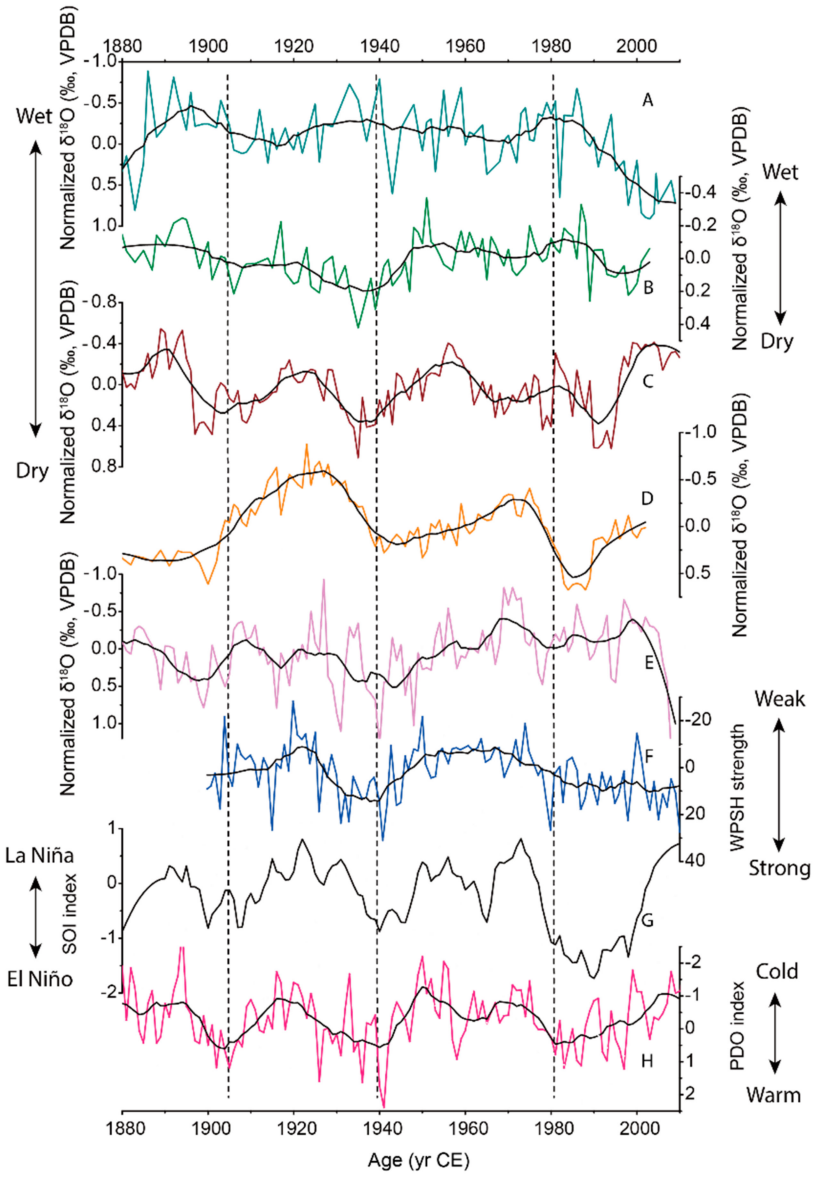

Figure 10. Normalized speleothem $\delta^{18}O$ records during the last 200 yrs and reconstructions of WPSH, ENSO and PDO variability. (**A**) Huangye [54], (**B**) Wanxiang [10], (**C**) Shihua [118], (**K**) Heshang [51] and (**E**) E'mei [44] cave $\delta^{18}O$ records in China. (**F**) WPSH strength (data from China National Climate Center); (**G**) Southern Oscillation Index (SOI, data from National Center for Atmospheric); (**H**) PDO index (data from Joint Institute for the Study of the Atmosphere and Ocean). The black lines in each panel are the 20 year running means.

High-resolution (1~3-year) records from SW China, SE China, central China, the eastern part of NW China and northern China [50,54,128] show a trend towards higher speleothem $\delta^{18}O$ during the 20th century (Figure 11). A similar trend is observed in solar irradiance [242] and global surface temperature anomaly [243,244] but drawing robust conclusions on the causal relationship between these variables is not straightforward. It is difficult, for example, to explain the observed EASM weakening trend during the 20th century in terms of solar irradiance (Figure 11a) and global surface temperature anomalies (Figure 11b) primarily because their increase would have enhanced the land-sea temperature gradient and thus strengthen (rather than weaken) the EASM, as shown by meteorological data. Anthropogenic forcing, such as that from aerosols, has been proposed to explain this trend [245], but further investigations are required to resolve the mechanisms underpinning these trends.

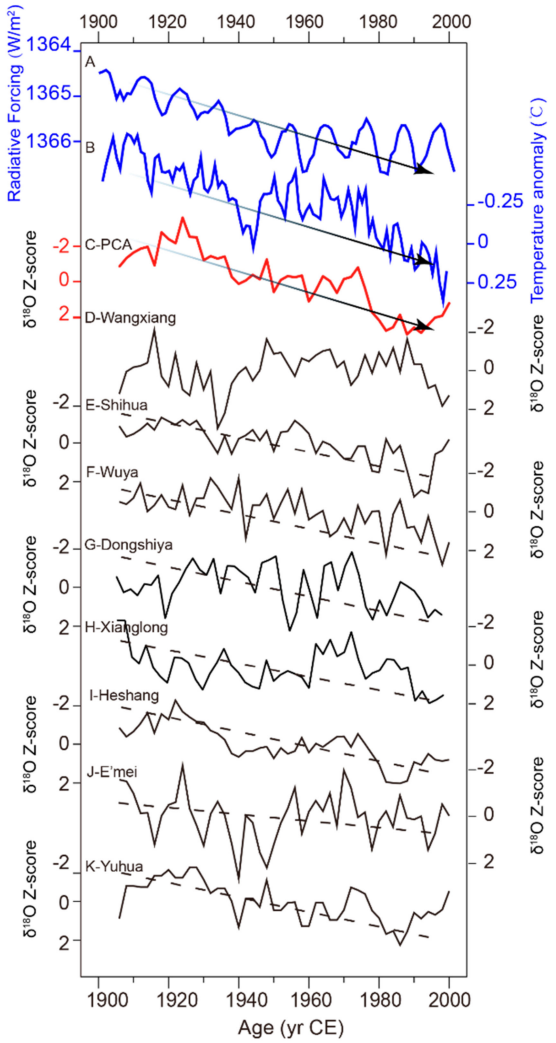

Figure 11. High-resolution speleothem $\delta^{18}O$ records from China with the solar radiation and global temperature curves for the 20th century. (**A**) Solar radiation [242]; (**B**) Temperature anomaly (data from National Centers for Environmental Information); (**C**) First Principal Component of the speleothem $\delta^{18}O$ records in (**D**–**K**); (**D**) Wanxiang Cave [10]; (E) Shihua Cave [128]; (**F**) Wuya Cave [150]; (**G**) Dongshiya Cave [50]; (**H**) Xianglong Cave [246]; (**I**) Heshang Cave [15]; (**J**) E'mei Cave [54] and (**K**) Yuhua Cave [178]. Speleothem records in (**D**–**K**) have resolutions higher than 2 years. Dotted lines in (**D**–**K**) show the long-term trend of each speleothem record. Principal Component Analysis has been done on speleothem $\delta^{18}O$ converted to standard Z-scores using the software Origin Pro 2016. All axes are reversed.

5. Conclusions

China has witnessed a rapid increase in the number of speleothem studies over the last 20 years, with more than 100 speleothem records from ~80 caves published in ~300 papers. Most studies attribute changes in speleothem $\delta^{18}O$ to variable EASM intensities. The longest records from southern and central China show that the Northern Hemisphere Summer Insolation is the main driver of EASM variability on orbital-scales. On millennial timescales, weak EASM events are causally linked to cold events in the North Atlantic in the late Pleistocene and to North Atlantic ice-rafting events during the Holocene. On centennial to decadal timescales, however, changes in monsoonal precipitation appear to be spatially heterogeneous due to a variable spatio-temporal distribution of the monsoonal rainfall belt in response to a complex geographical configuration. EASM is also significantly affected by the PDO, WPSH and ENSO modes, as well as solar activity. More efforts are required to produce

annual-decadal resolution $\delta^{18}O$ records with small dating uncertainties in China in combination with other climate proxies (e.g., trace element ratios) in particular in SE, NE and SW China. This, coupled with an increased availability of isotope-enabled climate simulations, would strengthen our ability to understand the mechanisms underpinning changes in speleothem $\delta^{18}O$ at various timescales.

Author Contributions: H.Z., H.C., Y.A.B., H.L. and J.Z. prepared the manuscript; H.Z., Y.A.B., H.L., J.Z., Y.T., J.W., F.Z. and Y.N. prepared the data; H.Z., H.L., J.Z., Y.A.B. and G.K. prepared the figures; J.B. and R.L.E. edited the manuscript; H.C. supervised this work. All authors contributed to the discussion of the manuscript.

Funding: The authors were supported by grants from the National Natural Science Foundation of China (41888101, 41502166, 41731174, 41703007), the China Postdoctoral Science Foundation (2015M580832, 2018M640971), U.S. National Science Foundation Grant 1702816 and 111 Project of China (D19002).

Acknowledgments: SISAL is a Working Group of PAGES program. We thank PAGES for their support for this activity. We especially thank the scientific editors Sandy P. Harrison and Laia Comas-Bru as well as three anonymous reviewers for their constructive comments and suggestions. We thank WOKAM (World Karst Aquifer Map) for providing the base karst map for the region and we thank Laia Comas-Bru for creating the code and generating Figures 1 and 3. Thanks also to Tingyong Li, Jinguo Dong, Jianjun Yin and Jiayi Liang for supplying the database from their groups.

Conflicts of Interest: The authors declare no conflict of interest.

References

1. Cheng, H.; Edwards, R.L.; Sinha, A.; Spötl, C.; Yi, L.; Chen, S.; Kelly, M.; Kathayat, G.; Wang, X.; Li, X.; et al. The Asian monsoon over the past 640,000 years and ice age terminations. *Nature* **2016**, *534*, 640–646. [CrossRef] [PubMed]
2. Cheng, H.; Sinha, A.; Wang, X.; Cruz, F.W.; Edwards, R.L. The Global Paleomonsoon as seen through speleothem records from Asia and the Americas. *Clim. Dyn.* **2012**, *39*, 1045–1062. [CrossRef]
3. Edwards, R.L.; Chen, J.; Wasserburg, G. $^{238}U^{234}U^{230}Th^{232}Th$ systematics and the precise measurement of time over the past 500,000 years. *Earth Planet. Sci. Lett.* **1987**, *81*, 175–192. [CrossRef]
4. Cheng, H.; Edwards, R.L.; Shen, C.-C.; Polyak, V.J.; Asmerom, Y.; Woodhead, J.; Hellstrom, J.; Wang, Y.; Kong, X.; Spötl, C. Improvements in ^{230}Th dating, ^{230}Th and ^{234}U half-life values, and U-Th isotopic measurements by multi-collector inductively coupled plasma mass spectrometry. *Earth Planet. Sci. Lett.* **2013**, *371*, 82–91. [CrossRef]
5. Wang, Y.; Cheng, H.; Edwards, R.; An, Z.; Wu, J.; Shen, C.; Dorale, J. A high-resolution absolute-dated late Pleistocene monsoon record from Hulu Cave, China. *Science* **2001**, *294*, 2345. [CrossRef]
6. Cruz, F.W., Jr.; Burns, S.J.; Jercinovic, M.; Karmann, I.; Sharp, W.D.; Vuille, M. Evidence of rainfall variations in Southern Brazil from trace element ratios (Mg/Ca and Sr/Ca) in a Late Pleistocene stalagmite. *Geochim. Cosmochim. Acta* **2007**, *71*, 2250–2263. [CrossRef]
7. Cheng, H.; Sinha, A.; Verheyden, S.; Nader, F.; Li, X.; Zhang, P.; Yin, J.; Yi, L.; Peng, Y.; Rao, Z. The climate variability in northern Levant over the past 20,000 years. *Geophys. Res. Lett.* **2015**, *42*, 8641–8650. [CrossRef]
8. Wang, Y.; Cheng, H.; Edwards, R.; He, Y.; Kong, X.; An, Z.; Wu, J.; Kelly, M.; Dykoski, C.; Li, X. The Holocene Asian monsoon: Links to solar changes and North Atlantic climate. *Science* **2005**, *308*, 854–857. [CrossRef] [PubMed]
9. Wang, Y.; Cheng, H.; Edwards, R.; Kong, X.; Shao, X.; Chen, S.; Wu, J.; Jiang, X.; Wang, X.; An, Z. Millennial-and orbital-scale changes in the East Asian monsoon over the past 224,000 years. *Nature* **2008**, *451*, 1090–1093. [CrossRef]
10. Zhang, P.; Cheng, H.; Edwards, R.; Chen, F.; Wang, Y.; Yang, X.; Liu, J.; Tan, M.; Wang, X. A test of climate, sun, and culture relationships from an 1810-year Chinese cave record. *Science* **2008**, *322*, 940–942. [CrossRef]
11. Cheng, H.; Edwards, R.L.; Broecker, W.S.; Denton, G.H.; Kong, X.; Wang, Y.; Zhang, R.; Wang, X. Ice age terminations. *Science* **2009**, *326*, 248–252. [CrossRef] [PubMed]
12. Yuan, D.; Cheng, H.; Edwards, R.; Dykoski, C.; Kelly, M.; Zhang, M.; Qing, J.; Lin, Y.; Wang, Y.; Wu, J. Timing, duration, and transitions of the last interglacial Asian monsoon. *Science* **2004**, *304*, 575–577. [CrossRef] [PubMed]

13. Cai, Y.; Fung, I.Y.; Edwards, R.L.; An, Z.; Cheng, H.; Lee, J.-E.; Tan, L.; Shen, C.-C.; Wang, X.; Day, J.A. Variability of stalagmite-inferred Indian monsoon precipitation over the past 252,000 y. *Proc. Natl. Acad. Sci. USA* **2015**, *112*, 2954–2959. [CrossRef] [PubMed]
14. Zhang, H.; Griffiths, M.L.; Chiang, J.C.; Kong, W.; Wu, S.; Atwood, A.; Huang, J.; Cheng, H.; Ning, Y.; Xie, S. East Asian hydroclimate modulated by the position of the westerlies during Termination I. *Science* **2018**, *362*, 580–583. [CrossRef] [PubMed]
15. Hu, C.; Henderson, G.; Huang, J.; Xie, S.; Sun, Y.; Johnson, K. Quantification of Holocene Asian monsoon rainfall from spatially separated cave records. *Earth Planet. Sci. Lett.* **2008**, *266*, 221–232. [CrossRef]
16. Comas-Bru, L.; Harrison, S.P. SISAL: Bringing added value to speleothem research. *Quaternary* **2019**, *2*, 7. [CrossRef]
17. Comas-Bru, L.; Harrison, S.P.; Werner, M.; Rehfeld, K.; Scroxton, N.; Veiga-Pires, C.; Members, S.W.G. Evaluating model outputs using integrated global speleothem records of climate change since the last glacial. *Clim. Past Discuss.* **2019**, *2019*, 1–53. [CrossRef]
18. Atsawawaranunt, K.; Harrison, S.; Comas Bru, L. *SISAL (Speleothem Isotopes Synthesis and Analysis Working Group) Database Version 1.0*; University of Reading: Redding, UK, 2018. [CrossRef]
19. Atsawawaranunt, K.; Comas-Bru, L.; Amirnezhad Mozhdehi, S.; Deininger, M.; Harrison, S.P.; Baker, A.; Boyd, M.; Kaushal, N.; Ahmad, S.M.; Ait Brahim, Y. The SISAL database: A global resource to document oxygen and carbon isotope records from speleothems. *Earth Syst. Sci. Data* **2018**. [CrossRef]
20. Kaushal, N.; Breitenbach, S.F.; Lechleitner, F.A.; Sinha, A.; Tewari, V.C.; Ahmad, S.M.; Berkelhammer, M.; Band, S.; Yadava, M.; Ramesh, R. The Indian Summer Monsoon from a Speleothem $\delta^{18}O$ Perspective—A Review. *Quaternary* **2018**, *1*, 29. [CrossRef]
21. Cheng, H.; Zhang, P.; Spötl, C.; Edwards, R.; Cai, Y.; Zhang, D.; Sang, W.; Tan, M.; An, Z. The climatic cyclicity in semiarid-arid central Asia over the past 500,000 years. *Geophys. Res. Lett.* **2012**, *39*. [CrossRef]
22. Cai, Y.; Chiang, J.C.; Breitenbach, S.F.; Tan, L.; Cheng, H.; Edwards, R.L.; An, Z. Holocene moisture changes in western China, Central Asia, inferred from stalagmites. *Quat. Sci. Rev.* **2017**, *158*, 15–28. [CrossRef]
23. Liu, X.; Rao, Z.; Shen, C.C.; Liu, J.; Chen, J.; Chen, S.; Wang, X.; Chen, F. Holocene solar activity imprint on centennial-to multidecadal-scale hydroclimatic oscillations in arid central Asia. *J. Geophys. Res. Atmos.* **2019**, *124*, 2562–2573. [CrossRef]
24. Cai, Y.; Cheng, H.; An, Z.; Edwards, R.; Wang, X.; Tan, L.; Wang, J. Large variations of oxygen isotopes in precipitation over south-central Tibet during Marine Isotope Stage 5. *Geology* **2010**, *38*, 243. [CrossRef]
25. Cai, Y.; Zhang, H.; Cheng, H.; An, Z.; Edwards, R.L.; Wang, X.; Tan, L.; Liang, F.; Wang, J.; Kelly, M. The Holocene Indian monsoon variability over the Southern Tibetan Plateau and its teleconnections. *Earth Planet. Sci. Lett.* **2012**, *335*, 135–144. [CrossRef]
26. Han, J.; Shao, Z.; Cheng, H.; Meng, X.; Wang, J.; Yu, J.; Yang, C.; Meng, Q.; Xu, B. Climate change since 7ka BP revealed by a high-resolution stalagmite $\delta^{18}O$ and $\delta^{13}C$ record from Benle Cave in Chamdo, Tibet. *Acta Geol. Sin.* **2017**, *91*, 2545–2556.
27. Bai, Y.; Zhang, P.; Gao, T.; Yu, R.; Zhou, P.; Cheng, H. The 5400 a BP extreme weakening event of the Asian summer monsoon and cultural evolution. *Sci. China Earth Sci.* **2017**, *60*, 1171–1182. [CrossRef]
28. Tan, L.; Cai, Y.; An, Z.; Cheng, H.; Shen, C.-C.; Breitenbach, S.F.; Gao, Y.; Edwards, R.L.; Zhang, H.; Du, Y. A Chinese cave links climate change, social impacts, and human adaptation over the last 500 years. *Sci. Rep.* **2015**, *5*, 12284. [CrossRef] [PubMed]
29. Tan, L.; Shen, C.-C.; Cai, Y.; Cheng, H.; Edwards, R.L. Great flood in the middle-lower Yellow River reaches at 4000 a BP inferred from accurately-dated stalagmite records. *Sci. Bull.* **2018**, *63*, 206–208. [CrossRef]
30. Chen, Z.; Auler, A.S.; Bakalowicz, M.; Drew, D.; Griger, F.; Hartmann, J.; Jiang, G.; Moosdorf, N.; Richts, A.; Stevanovic, Z. The World Karst Aquifer Mapping project: Concept, mapping procedure and map of Europe. *Hydrogeol. J.* **2017**, *25*, 771–785. [CrossRef]
31. Ding, Y.; Chan, J.C. The East Asian summer monsoon: An overview. *Meteorol. Atmos. Phys.* **2005**, *89*, 117–142.
32. Wang, B.; Lin, H. Rainy season of the Asian–Pacific summer monsoon. *J. Clim.* **2002**, *15*, 386–398. [CrossRef]
33. Tao, S.Y.; Chen, L. A review of recent research on the East Asian summer monsoon in China. In *Monsoon Meteorology*; Chang, C., Krishnamurti, T., Eds.; Oxford University Press: London, UK, 1987; pp. 60–92.
34. Chiang, J.C.; Fung, I.Y.; Wu, C.-H.; Cai, Y.; Edman, J.P.; Liu, Y.; Day, J.A.; Bhattacharya, T.; Mondal, Y.; Labrousse, C.A. Role of seasonal transitions and westerly jets in East Asian paleoclimate. *Quat. Sci. Rev.* **2015**, *108*, 111–129. [CrossRef]

35. Kong, W.; Swenson, L.M.; Chiang, J.C. Seasonal transitions and the westerly jet in the Holocene East Asian summer monsoon. *J. Clim.* **2017**, *30*, 3343–3365. [CrossRef]
36. Li, Y.; Morrill, C. A Holocene East Asian winter monsoon record at the southern edge of the Gobi Desert and its comparison with a transient simulation. *Clim. Dyn.* **2015**, *45*, 1219–1234. [CrossRef]
37. Kurita, N.; Yoshida, N.; Inoue, G.; Chayanova, E.A. Modern isotope climatology of Russia: A first assessment. *J. Geophys. Res. Atmos.* **2004**, *109*. [CrossRef]
38. Becker, A.; Finger, P.; Meyer-Christoffer, A.; Rudolf, B.; Ziese, M. GPCC full data reanalysis version 6.0 at 1.0°: Monthly land-surface precipitation from rain-gauges built on GTS-based and historic data. *Glob. Precip. Climatol. Cent. (Gpcc) Berl. Ger.* **2011**. [CrossRef]
39. Rienecker, M.M.; Suarez, M.J.; Gelaro, R.; Todling, R.; Bacmeister, J.; Liu, E.; Bosilovich, M.G.; Schubert, S.D.; Takacs, L.; Kim, G.-K. MERRA: NASA's modern-era retrospective analysis for research and applications. *J. Clim.* **2011**, *24*, 3624–3648. [CrossRef]
40. Chen, F.-H.; Chen, J.-H.; Holmes, J.; Boomer, I.; Austin, P.; Gates, J.B.; Wang, N.-L.; Brooks, S.J.; Zhang, J.-W. Moisture changes over the last millennium in arid central Asia: A review, synthesis and comparison with monsoon region. *Quat. Sci. Rev.* **2010**, *29*, 1055–1068. [CrossRef]
41. Wu, J.; Wang, Y.; Kong, X. Evolution and abrupt changes of the Holocene Asian monsoon climate recorded by stalagmite in Baigu Cave in Guizhou. *Mar. Geol. Quat. Geol.* **2006**, *26*, 55–60.
42. Jiang, X.; He, Y.; Shen, C.-C.; Li, Z.; Lin, K. Replicated stalagmite-inferred centennial-to decadal-scale monsoon precipitation variability in southwest China since the mid Holocene. *Holocene* **2013**, *23*, 841–849. [CrossRef]
43. Zhao, K.; Wang, Y.; Edwards, R.L.; Cheng, H.; Liu, D. High-resolution stalagmite $\delta^{18}O$ records of Asian monsoon changes in central and Southern China spanning the MIS 3/2 transition. *Earth Planet. Sci. Lett.* **2010**, *298*, 191–198. [CrossRef]
44. Tan, L.; Cai, Y.; Cheng, H.; An, Z.; Edwards, R.L. Summer monsoon precipitation variations in central China over the past 750 years derived from a high-resolution absolute-dated stalagmite. *Palaeogeogr. Palaeoclimatol. Palaeoecol.* **2009**, *280*, 432–439. [CrossRef]
45. Dykoski, C.A.; Edwards, R.L.; Cheng, H.; Yuan, D.; Cai, Y.; Zhang, M.; Lin, Y.; Qing, J.; An, Z.; Revenaugh, J. A high-resolution, absolute-dated Holocene and deglacial Asian monsoon record from Dongge Cave, China. *Earth Planet. Sci. Lett.* **2005**, *233*, 71–86. [CrossRef]
46. Zhao, K.; Wang, Y.; Edwards, R.L.; Cheng, H.; Liu, D.; Kong, X. A high-resolved record of the Asian Summer Monsoon from Dongge Cave, China for the past 1200 years. *Quat. Sci. Rev.* **2015**, *122*, 250–257. [CrossRef]
47. Duan, F.; Wang, Y.; Shen, C.-C.; Wang, Y.; Cheng, H.; Wu, C.-C.; Hu, H.-M.; Kong, X.; Liu, D.; Zhao, K. Evidence for solar cycles in a late Holocene speleothem record from Dongge Cave, China. *Sci. Rep.* **2014**, *4*, 5159. [CrossRef] [PubMed]
48. He, Y.; Wang, Y.; Kong, X.; Cheng, H. High resolution stalagmite $\delta^{18}O$ records over the past 1000 years from Dongge Cave in Guizhou. *Chin. Sci. Bull.* **2005**, *50*, 1003. [CrossRef]
49. Zhu, X.; Zhang, M.; Lin, Y.; Qin, J.; Yang, Y. Carbon isotopic records from stalagmites and the signification of paleo-ecological environment in the area of Guangxi—Guizhou, China. *Environ. Geol.* **2006**, *51*, 267–273. [CrossRef]
50. Zhao, J.; Cheng, H.; Yang, Y.; Tan, L.; Spötl, C.; Ning, Y.; Zhang, H.; Cheng, X.; Sun, Z.; Li, X. Reconstructing the western boundary variability of the Western Pacific Subtropical High over the past 200 years via Chinese cave oxygen isotope records. *Clim. Dyn.* **2019**, *52*, 3741–3757. [CrossRef]
51. Zhang, N.; Yang, Y.; Cheng, H.; Zhao, J.; Yang, X.; Liang, S.; Nie, X.; Zhang, Y.; Edwards, R.L. Timing and duration of the East Asian summer monsoon maximum during the Holocene based on stalagmite data from North China. *Holocene* **2018**, *28*, 1631–1641. [CrossRef]
52. Dong, J.; Shen, C.-C.; Kong, X.; Wang, Y.; Duan, F. Asian monsoon dynamics at Dansgaard/Oeschger events 14–8 and Heinrich events 5–4 in Northern China. *Quat. Geochronol.* **2018**, *47*, 72–80. [CrossRef]
53. Wan, N.; Chung, W.; Li, H.-C.; Lin, H.; Ku, T.-L.; Shen, C.-C.; Yuan, D.; Zhang, M.; Lin, Y. Comparison of speleothem $\delta^{18}O$ records from eastern China with solar insolation, ice core and marine records: Similarities and discrepancies on different time scales. *J. Asian Earth Sci.* **2011**, *40*, 1151–1163. [CrossRef]
54. Zhang, H.; Cheng, H.; Spötl, C.; Cai, Y.; Sinha, A.; Tan, L.; Yi, L.; Yan, H.; Kathayat, G.; Ning, Y.; et al. A 200-year annually laminated stalagmite record of precipitation seasonality in southeastern China and its linkages to ENSO and PDO. *Sci. Rep.* **2018**, *8*, 12344. [CrossRef] [PubMed]

55. Li, H.-C.; Bar-Matthews, M.; Chang, Y.-P.; Ayalon, A.; Yuan, D.-X.; Zhang, M.-L.; Lone, M.A. High-resolution $\delta^{18}O$ and $\delta^{13}C$ records during the past 65 ka from Fengyu Cave in Guilin: Variation of monsoonal climates in south China. *Quat. Int.* **2017**, *441*, 117–128. [CrossRef]
56. Li, T.-Y.; Shen, C.-C.; Li, H.-C.; Li, J.-Y.; Chiang, H.-W.; Song, S.-R.; Yuan, D.-X.; Lin, C.D.-J.; Gao, P.; Zhou, L. Oxygen and carbon isotopic systematics of aragonite speleothems and water in Furong Cave, Chongqing, China. *Geochim. Cosmochim. Acta* **2011**, *75*, 4140–4156. [CrossRef]
57. Li, H.-C.; Lee, Z.-H.; Wan, N.-J.; Shen, C.-C.; Li, T.-Y.; Yuan, D.-X.; Chen, Y.-H. The $\delta^{18}O$ and $\delta^{13}C$ records in an aragonite stalagmite from Furong Cave, Chongqing, China: A-2000-year record of monsoonal climate. *J. Asian Earth Sci.* **2011**, *40*, 1121–1130. [CrossRef]
58. Zhang, H.; Griffiths, M.L.; Huang, J.; Cai, Y.; Wang, C.; Zhang, F.; Cheng, H.; Ning, Y.; Hu, C.; Xie, S. Antarctic link with East Asian summer monsoon variability during the Heinrich Stadial–Bølling interstadial transition. *Earth Planet. Sci. Lett.* **2016**, *453*, 243–251. [CrossRef]
59. Jiang, W.; Zhao, K.; Chen, S.; Wang, Y.; Cheng, H.; Ning, Y. Decadal climate oscillations during the Little Ice Age of stalagmite record from Heizhugou Cave, Sichuan. *Quat. Sci.* **2017**, *37*, 118–129.
60. Cui, Y.; Wang, Y.; Cheng, H.; Zhao, K.; Kong, X. Isotopic and lithologic variations of one precisely-dated stalagmite across the Medieval/LIA period from Heilong Cave, central China. *Clim. Past* **2012**, *8*, 1541–1550. [CrossRef]
61. Liu, Y.; Henderson, G.; Hu, C.; Mason, A.; Charnley, N.; Johnson, K.; Xie, S. Links between the East Asian monsoon and North Atlantic climate during the 8200 year event. *Nat. Geosci.* **2013**, *6*, 117–120. [CrossRef]
62. Yang, X.; Zhang, P.; Chen, F.; Huh, C.; Li, H.; Cheng, H.; Johnson, K.R.; Liu, J.; An, C. Modern stalagmite oxygen isotopic composition and its implications of climatic change from a high-elevation cave in the eastern Qinghai-Tibet Plateau over the past 50 years. *Chin. Sci. Bull.* **2007**, *52*, 1238–1247. [CrossRef]
63. Tan, L.; Cai, Y.; An, Z.; Edwards, R.L.; Cheng, H.; Shen, C.C.; Zhang, H. Centennial-to decadal-scale monsoon precipitation variability in the semi-humid region, Northern China during the last 1860 years: Records from stalagmites in Huangye Cave. *Holocene* **2010**, *21*, 287–296.
64. Cheng, H.; Edwards, R.L.; Southon, J.; Matsumoto, K.; Feinberg, J.M.; Sinha, A.; Zhou, W.; Li, H.; Li, X.; Xu, Y. Atmospheric 14C/12C changes during the last glacial period from Hulu Cave. *Science* **2018**, *362*, 1293–1297. [CrossRef] [PubMed]
65. Wang, Y.; Wu, J.; Liu, D.; Wu, J.; Cai, Y.; Cheng, H. A quick cooling event of the East Asian monsoon responding to heinrich event 1: Evidence from stalagmite $\delta^{18}O$ records. *Sci. China Ser. D Earth Sci.* **2002**, *45*, 88. [CrossRef]
66. Kong, X.; Wang, Y.; Wu, J.; Cheng, H. A continuous 3000-year precipitation record of ENSO variability during LGM from a stalagmite in Nanjing. *Chin. Sci. Bull.* **2003**, *48*, 480–484. [CrossRef]
67. Zhang, W.; Wang, Y.; Wu, J.; Duan, F. Last deglacial climate variations inferred from trace elements in a stalagmite from Hulu Cave, Nanjing. *Quat. Sci.* **2014**, *34*, 1227–1237.
68. Wu, J.; Wang, Y.; Cheng, H.; Edwards, R.L. An exceptionally strengthened East Asian summer monsoon event between 19.9 and 17.1 ka BP recorded in a Hulu stalagmite. *Sci. China Ser. D Earth Sci.* **2009**, *52*, 360–368. [CrossRef]
69. Wang, Q.; Wang, Y.; Shao, Q.; Liang, Y.; Zhang, Z.; Kong, X. Millennial-scale Asian monsoon variability during the late Marine Isotope Stage 6 from Hulu Cave, China. *Quat. Res.* **2018**, *90*, 394–405. [CrossRef]
70. Cheng, H.; Edwards, R.; Wang, Y.; Kong, X.; Ming, Y.; Kelly, M.; Wang, X.; Gallup, C.; Liu, W. A penultimate glacial monsoon record from Hulu Cave and two-phase glacial terminations. *Geology* **2006**, *34*, 217. [CrossRef]
71. Duan, F.; Wu, J.; Wang, Y.; Edwards, R.L.; Cheng, H.; Kong, X.; Zhang, W. A 3000-yr annually laminated stalagmite record of the Last Glacial Maximum from Hulu Cave, China. *Quat. Res.* **2015**, *83*, 360–369. [CrossRef]
72. Wu, J.; Shao, X.; Kong, X.; Wang, Y. Imprint of solar activity on Nanjing stalagmite annual layer thickness sequence during the Last Glacial Maximum. *Chin. Sci. Bull.* **2006**, *51*, 441–447. [CrossRef]
73. Xia, Z.; Wang, Y.; Wu, J. The Evolution of ENSO during LGM from Precipitation Record in Nanjing. *J. Nanjing Norm. Univ. (Nat. Sci.)* **2006**, *29*, 106–110.
74. Cosford, J.; Qing, H.; Lin, Y.; Eglington, B.; Mattey, D.; Chen, Y.G.; Zhang, M.; Cheng, H. The East Asian monsoon during MIS 2 expressed in a speleothem $\delta^{18}O$ record from Jintanwan Cave, Hunan, China. *Quat. Res.* **2010**, *73*, 541–549. [CrossRef]

75. Cai, Y.; Tan, L.; Cheng, H.; An, Z.; Edwards, R.L.; Kelly, M.J.; Kong, X.; Wang, X. The variation of summer monsoon precipitation in central China since the last deglaciation. *Earth Planet. Sci. Lett.* **2010**, *291*, 21–31. [CrossRef]
76. Wang, Q.; Zhou, H.; Cheng, K.; Chi, H.; Shen, C.-C.; Wang, C.; Ma, Q. The climate reconstruction in Shandong Peninsula, Northern China, during the last millennium based on stalagmite laminae together with a comparison to δ^{18}O. *Clim. Past* **2016**, *12*, 871–881. [CrossRef]
77. Ma, Z.-B.; Cheng, H.; Tan, M.; Edwards, R.L.; Li, H.-C.; You, C.-F.; Duan, W.-H.; Wang, X.; Kelly, M.J. Timing and structure of the Younger Dryas event in Northern China. *Quat. Sci. Rev.* **2012**, *41*, 83–93. [CrossRef]
78. Duan, W.; Tan, M.; Ma, Z.; Cheng, H. The palaeoenvironmental significance of δ^{13}C of stalagmite BW-1 from Beijing, China during Younger D ryas intervals inferred from the grey level profile. *Boreas* **2014**, *43*, 243–250. [CrossRef]
79. Li, S.; Yang, Y.; Li, T.; Ma, R.; Guo, Y. Asian Monsoonal Climate Variability at Orbital Scales during the MIS8—MIS9: Based on Stalagmite Data from Laomu Cave, Henan Province, China. *Geol. Rev.* **2011**, *57*, 754–760.
80. Yin, J.-J.; Yuan, D.-X.; Li, H.-C.; Cheng, H.; Li, T.-Y.; Edwards, R.; Lin, Y.-S.; Qin, J.-M.; Tang, W.; Zhao, Z.-Y. Variation in the Asian monsoon intensity and dry-wet conditions since the Little Ice Age in central China revealed by an aragonite stalagmite. *Clim. Past* **2014**, *10*, 1803–1816. [CrossRef]
81. Zhang, H.-L.; Yu, K.-F.; Zhao, J.-X.; Feng, Y.-X.; Lin, Y.-S.; Zhou, W.; Liu, G.-H. East Asian Summer Monsoon variations in the past 12.5 ka: High-resolution δ^{18}O record from a precisely dated aragonite stalagmite in central China. *J. Asian Earth Sci.* **2013**, *73*, 162–175. [CrossRef]
82. Dong, J.; Shen, C.-C.; Kong, X.; Wang, H.-C.; Jiang, X. Reconciliation of hydroclimate sequences from the Chinese Loess Plateau and low-latitude East Asian Summer Monsoon regions over the past 14,500 years. *Palaeogeogr. Palaeoclimatol. Palaeoecol.* **2015**, *435*, 127–135. [CrossRef]
83. Li, Q.; Li, G.; Chen, M.-T.; Cheng, H.; Xu, J.; Ding, D.; Ma, Y.; Qiao, L.; Zhang, Q.; Zhang, Y. East Asian summer monsoon variations during the last deglaciation, recorded from a stalagmite at Linyi, Northern China. *Quat. Int.* **2017**, *464*, 327–335. [CrossRef]
84. Zhao, C.; Wang, Z.; Tao, K.; Wang, J.; Lin, Y.; Zhang, M. Reconstruction of the Paleoclimate and Paleoenvironment of a Stalagmite from Longuan Cave, Guizhou between 1600~250 a. **2004**, *26*, 209–2014.
85. Wang, L.; Zhao, K.; Huang, W.; Zhang, W.; Shao, Q.; Wang, Y. Centennial-scale monsoon failure during the Younger Dryas event record in a high-resolution stalagmite from Longfugong Cave, central China. *J. Nanjing Norm. Univ. (Nat. Sci.)* **2017**, *40*, 134–143.
86. Mao, R.; Cai, Y.; Ma, L.; Cheng, X. Early to mid-Holocene paleoclimatic changes recorded by the stalagmites from the Madou Cave, Henan Provience. *J. Earth Environ.* **2016**, *7*, 254–268.
87. Yin, J.; Tng, W. The Relationship between Local Climate/Large Scale Circulation and δ^{18}O Recorded by Stalagmite in the Past 50 Years from Maomaotou Big Cave, Guilin. *Acta Geol. Sin.* **2016**, *90*, 2035–2042.
88. Zhao, K.; Wang, Y.; Edwards, R.L.; Cheng, H.; Liu, D.; Kong, X.; Ning, Y. Contribution of ENSO variability to the East Asian summer monsoon in the late Holocene. *Palaeogeogr. Palaeoclimatol. Palaeoecol.* **2016**, *449*, 510–519. [CrossRef]
89. Wu, J.; Wang, Y.; Dong, J. Changes in East Asian summer monsoon during the Holocene recorded by stalagmite δ^{18}O records from Liaoning province. *Quat. Sci.* **2011**, *31*, 990–998.
90. Zhang, W.; Wu, J. Ecological response of δ^{13}C to Holocene climate changes from stalagmite record in Nuanhe Cave, Liaoning. *Mar. Geol. Quat. Geol.* **2012**, *32*, 147–154. [CrossRef]
91. Dong, J. Summer monsoon precipitation variations and abrupt climate events during the 3000 years: Records from stalagmites in China. *J. Arid Land Resour. Environ.* **2012**, *26*, 36–41.
92. Gu, N.; Wu, J. Paleoclimate significance of δ^{13}C in stalagmite from Nuanhe Cave, Liaoning. *Carsologica Sin.* **2012**, *31*, 107–114.
93. Guo, Y.; Wu, J.; Wang, Y.; Dong, J. Early Holocene laminated stalagmite records from Nunehe Cave, Benxi, China. *Mar. Geol. Quat. Geol.* **2012**, *32*, 135–141. [CrossRef]
94. Qin, J.; Yuan, D.; Lin, Y.; Zhang, M.; Li, B. Isotopic records of stalagmites from Guilin since 44 ka BP and their environmental interpretation. *Acta Geosci. Sin.* **2000**, *21*, 407–416.
95. Li, M.; Wang, Y.; Qiu, Q. High Resolution Stalagmite Records of East Asian Monsoon from 7 to 6 ka BP in Mid-Holocene. *Sci. Geogr. Sin.* **2007**, *27*, 519–524.

96. Liang, Y.; Kong, X.; Wang, Y. The relationship between annual laminae and stable isotopes in two stalagmites in Shennongjia, Hubei. *Carsologica Sin.* **2008**, *27*, 371–376.
97. Xie, Y.; Wang, Y.; Jiang, X. Decadal-scale climate change of east asian monsoon during the Last Glacial Maximum from stalagimte record. *Mar. Geol. Quat. Geol.* **2008**, *28*, 43–49.
98. Zhang, W.; Wu, J.; Wang, Y.; Wang, Y.; Cheng, H.; Kong, X.; Duan, F. A detailed East Asian monsoon history surrounding the 'Mystery Interval'derived from three Chinese speleothem records. *Quat. Res.* **2014**, *82*, 154–163. [CrossRef]
99. Liu, D.; Wang, Y.; Cheng, H.; Edwards, R.; Kong, X.; Wang, X.; Wu, J. A detailed comparison of Asian Monsoon intensity and Greenland temperature during the Aller d and Younger Dryas events. *Earth Planet. Sci. Lett.* **2008**, *272*, 691–697. [CrossRef]
100. Liu, D.; Wang, Y.; Cheng, H.; Kong, X.; Chen, S. Centennial-scale Asian monsoon variability during the mid-Younger Dryas from Qingtian Cave, central China. *Quat. Res.* **2013**, *80*, 199–206. [CrossRef]
101. Wang, Q.; Liu, D.; Wang, Y.; Deng, C. Transitional patterns of YD and 8.2 ka event recorded by annually-laminated stalagmites from Qingtian Cave, Mt. Shennongjia. *Acta Sedimentol. Sin.* **2015**, *33*, 1140–1148.
102. Zhang, Z.; Liu, D.; Wang, Y.; Wagn, Q. Annual-to decadal-scale variability of Asian monsoon climates during Mid-Holocene: Evidence from proxies of annual bands and geochemical behaviors of a speleothem from 5.56 ka BP to 4.84 ka BP in Qingtian Cave, central China. *Quat. Sci.* **2014**, *34*, 1246–1255.
103. Wang, Q.; Wang, Y.; Liu, D.; Zhao, K.; Shao, Q.; Cheng, H.; Huang, W. The DO3 event in Asian monsoon climates evidenced by an annually laminated stalagmite from Qingtian Cave, Mt. Shennongjia. *Quat. Sci.* **2017**, *37*, 108–117.
104. Qiu, Q.; Wang, Y. The characteristics of climatic transition from Allerød to early Younger Dryas. *Mar. Geol. Quat. Geol.* **2007**, *27*, 107–112.
105. Liu, D.; Wang, Y.; Cheng, H.; Edwards, R.; Kong, X. Cyclic changes of Asian monsoon intensity during the early mid-Holocene from annually-laminated stalagmites, central China. *Quat. Sci. Rev.* **2015**, *121*, 1–10. [CrossRef]
106. Deng, C.; Wang, Y.; Liu, D.; Zhang, Z. The Asian monsoon variability around 8.2 ka recorded by an annually-laminated stalagmite from Mt. Shennongjia, central China. *Quat. Sci.* **2013**, *33*, 945–953.
107. Liu, D.; Wang, Y.; Cheng, H.; Edwards, R.; Kong, X.; Chen, S.; Liu, S. Contrasting patterns in abrupt Asian summer monsoon changes in the last glacial period and the Holocene. *Paleoceanogr. Paleoclimatol.* **2018**. [CrossRef]
108. Cai, Y.; Peng, Z.; An, Z.; Zhang, Z.; Cao, Y. The $\delta^{18}O$ variation of a stalagmite from Qixing Cave, Guizhou Province and indicated climate change during the Holocene. *Chin. Sci. Bull.* **2001**, *46*, 1904–1908. [CrossRef]
109. Ma, L.; Cai, Y.; Qin, S. A high resolution paleoclimate record of the last 2300 years in stalagmite QX-3 from the Qixing Cave, Guizhou Province. *J. Earth Environ.* **2015**, *6*, 135–144.
110. Qin, J.; Lin, Y.; Zhang, M.; Wang, H.; Feng, Y.; Tu, L. Change of the East-Asian monsoon climate during the Last Glaciation: $\delta^{18}O$ record of stalagmites in Qixing Cave, Duyun city, Guizhou Province. *Carsologica Sin.* **2003**, *22*, 167–173.
111. Qin, J.; Yuan, D.; Cheng, H.; Lin, Y.; Zhang, M.; Zhang, C.; Wang, F.; Wang, H.; Feng, Y.; Tu, L. A millennial scale climatic changes of eastern Asian monsoon in the past 250,000 years in Guizhou and Guangxi, China. *Carsologica Sin.* **2004**, *23*, 261–266.
112. Zhang, Z.-Q.; Wang, Y.-J.; Liu, D.-B.; Cheng, H.; Huang, W.; Wang, Q.; Liang, Y.-J. Multi-scale variability of the Asian monsoon recorded in an annually-banded stalagmite during the Neoglacial from Qixing Cave, Southwestern China. *Quat. Int.* **2018**, *487*, 78–86. [CrossRef]
113. Dong, J.; Wang, Y.; Cheng, H. A high-resolution stalagmite record of the Holocene East Asian monsoon from Mt Shennongjia, central China. *Holocene* **2010**, *20*, 257–264. [CrossRef]
114. Shao, X.; Wang, Y.; Cheng, H.; Kong, X.; Wu, J.; Edwards, R.L. Long-term trend and abrupt events of the Holocene Asian monsoon inferred from a stalagmite $\delta^{18}O$ record from Shennongjia in Central China. *Chin. Sci. Bull.* **2006**, *51*, 221–228. [CrossRef]
115. Dong, J.; Diao, W.; Kong, X. Variation in uranium isotopes of stalagmites from Sanbao Cave, Hubei province: Implications for palaeoclimate. *Mar. Geol. Quat. Geol.* **2013**, *33*, 129–135. [CrossRef]
116. Dong, J.; Kong, X.; Wang, Y. The East Asian monsoon clilmate changes at Mt. Shennongjia and its relation to shift of Intertropical Convergence Zone during the Holocene. *Quat. Sci.* **2006**, 827–834.

117. Xia, Z.; Kong, X.; Jiang, X.; Cheng, H. Precise dating of East-Asian-Monsoon D/O events during 95–56 ka BP: Based on stalagmite data from Shanbao Cave at Shennongjia, China. *Sci. China Ser. D Earth Sci.* **2007**, *50*, 228–235. [CrossRef]
118. Jiang, X.; Kong, X.; Wang, Y.; Cheng, H.; Wu, J.; Chen, S. Orbital-and millennial-scale variability of the Asian monsoon during MIS8 from Sanbao Cave at Mount Shennongjia, central China. *Chin. Sci. Bull.* **2010**, *55*, 1041–1046. [CrossRef]
119. Jiang, X.; Wang, X.; He, Y.; Hu, H.-M.; Li, Z.; Spötl, C.; Shen, C.-C. Precisely dated multidecadally resolved Asian summer monsoon dynamics 113.5–86.6 thousand years ago. *Quat. Sci. Rev. 143*, 1–12. [CrossRef]
120. Jiang, X.; He, Y.; Shen, C.-C.; Lee, S.-Y.; Yang, B.; Lin, K.; Li, Z. Decoupling of the East Asian summer monsoon and Indian summer monsoon between 20 and 17 ka. *Quat. Res.* **2014**, *82*, 146–153. [CrossRef]
121. Jiang, X.; He, Y.; Wang, X.; Dong, J.; Li, Z.; Lone, M.A.; Shen, C.-C. Sub-decadally-resolved Asian monsoon dynamics during Chinese interstadial 21 in response to northern high-latitude climate. *J. Asian Earth Sci.* **2018**, *172*, 243–248. [CrossRef]
122. Zhang, H.; Cheng, H.; Cai, Y.; Spötl, C.; Kathayat, G.; Sinha, A.; Edwards, R.L.; Tan, L. Hydroclimatic variations in southeastern China during the 4.2 ka event reflected by stalagmite records. *Clim. Past* **2018**, *14*, 1805–1817. [CrossRef]
123. Zhang, H.; Cai, Y.; Tan, L.; Cheng, H.; Qin, S.; An, Z.; Edwards, R.L.; Ma, L. Large variations of $\delta^{13}C$ values in stalagmites from southeastern China during historical times: Implications for anthropogenic deforestation. *Boreas* **2015**, *44*, 511–525. [CrossRef]
124. Zhang, H.; Cai, Y.; Tan, L.; Qin, S.; An, Z. Stable isotope composition alteration produced by the aragonite-to-calcite transformation in speleothems and implications for paleoclimate reconstructions. *Sediment. Geol.* **2014**, *309*, 1–14. [CrossRef]
125. Jiang, X.; He, Y.; Shen, C.; Kong, X.; Li, Z.; Chang, Y. Stalagmite-inferred Holocene precipitation in Northern Guizhou Province, China, and asynchronous termination of the Climatic Optimum in the Asian monsoon territory. *Chin. Sci. Bull.* **2012**, *57*, 795–801. [CrossRef]
126. Yang, B.; Lei, G.; Jiang, X. 9.9~4.2 ka BP stalagmite trace elements records from Shigao Cave, Northern Guizhou province and its environmental significance. *Mar. Geol. Quat. Geol.* **2014**, *34*, 143–148.
127. Tan, M.; Liu, T.; Hou, J.; Qin, X.; Zhang, H.; Li, T. Cyclic rapid warming on centennial-scale revealed by a 2650-year stalagmite record of warm season temperature. *Geophys. Res. Lett.* **2003**, *30*, 1617–1620. [CrossRef]
128. Li, X.; Cheng, H.; Tan, L.; Ban, F.; Sinha, A.; Duan, W.; Li, H.; Zhang, H.; Ning, Y.; Kathayat, G. The East Asian summer monsoon variability over the last 145 years inferred from the Shihua Cave record, North China. *Sci. Rep.* **2017**, *7*, 7078. [CrossRef] [PubMed]
129. Li, H.; Gu, D.; Ku, T.; Stott, L.; Chen, W. Applications of interannual-resolution stable isotope records of speleothem: Climatic changes in Beijing and Tianjin, China during the past 500 years—The $\delta^{18}O$ record. *Sci. China Ser. D Earth Sci.* **1998**, *41*, 362–368. [CrossRef]
130. Hou, J.; Tan, M.; Cheng, H.; Liu, T. Stable isotope records of plant cover change and monsoon variation in the past 2200 years: Evidence from laminated stalagmites in Beijing, China. *Boreas* **2003**, *32*, 304–313. [CrossRef]
131. Huang, J.; Chen, L.; Chen, Q.; Liu, S.; Yang, L.; Mi, X.; Deng, X.; Peng, X.; Li, H.; Zhou, H. The high-resolution speleothem $\delta^{13}C$ record during 54~46 ka from the Shizi Cave in NE Sichuan, Central China and influencing factors. *Geochimica* **2016**, *4*, 8.
132. Zhou, H.; Zhao, J.; Qing, W.; Feng, Y.; Tang, J. Speleothem-derived Asian summer monsoon variations in Central China, 54–46 ka. *J. Quat. Sci.* **2011**, *26*, 781–790. [CrossRef]
133. Zhang, M.; Lin, Y. Ages and stable isotopic measurements of No.1 stalagmite from Shuihan Cave in Guilin and their paleoclimatic inplications. *Geol. Geochem.* **2000**, *28*, 41–47.
134. Hou, J.; Tan, M.; Liu, D. Counting chronology and climate records with about 1000 annual layers of a Holocene stalagmite from the Water Cave in Liaoning Province, Chinaannual layers of a Holocene stalagmite from the Water Cave in Liaoning Province, China. *Sci. China Ser. D Earth Sci.* **2002**, *45*, 385–391. [CrossRef]
135. Liu, S.; Yang, L.; Huang, J.; Chen, L.; Chen, Q.; Mi, X.; He, H.; Zhou, H. A high-resolution speleothem $\delta^{13}C$ record from Songjia Cave in NE Sichuan, Central China and D/O event 5 to 10. *Geochimica* **2015**, *44*, 413–420.
136. Cao, Y.; Li, J.; Tang, J. Abrupt change analyses of oxygen, carbon isotope values and Sr contents in a stalagmite retrieved from Songjia Cave, NE Sichuan. *J. Anqing Teach. Coll. (Nat. Sci. Ed.)* **2012**, *18*, 88–90, 103.
137. Tang, J.; Cao, Y.; Zhou, H. Periodicity analyses of oxygen and carbon isotopes of a stalagmite retrieved from Songjia Cave, NE Sichuan in Central China. *J. Anqing Teach. Coll. (Nat. Sci. Ed.)* **2012**, *18*, 91–92, 97.

138. Mi, X.; Liu, S.; Chen, Q.; Zhao, J.; Zhou, H. High-resolution paleoclimate records of MIS9 in northeastern Sichuan, Central China. *Mar. Geol. Quat. Geol.* **2017**, *37*, 102–106.
139. Zhou, H.; Zhao, J.; Feng, Y.; Gagan, M.K.; Zhou, G.; Yan, J. Distinct climate change synchronous with Heinrich event one, recorded by stable oxygen and carbon isotopic compositions in stalagmites from China. *Quat. Res.* **2008**, *69*, 306–315. [CrossRef]
140. Liu, S.; Huang, J.; Chen, L.; Yang, L.; Chen, Q.; Mi, X.; He, H.; Deng, X.; Li, H.; Zhou, H. A Speleothem $\delta^{13}C$ Record and Control Mechanism during 120~103ka BP from NE Sichuan, Central China. *Acta Geol. Sin.* **2016**, *90*, 334–340.
141. Zhao, J.X.; Wang, Y.J.; Collerson, K.D.; Gagan, M.K. Speleothem U-series dating of semi-synchronous climate oscillations during the last deglaciation. *Earth Planet. Sci. Lett.* **2003**, *216*, 155–161. [CrossRef]
142. Jiang, X.; Li, Z.; Shen, C.; Li, J. 2100~590 aBP stalagmite stable isotope records from Tian'e cave and their regional climate significance. *Mar. Geol. Quat. Geol.* **2011**, *3*, 019. [CrossRef]
143. Chen, S.; Wang, Y.; Wu, J.; Liu, D. An event of the East Asian monsoon responding to Heinrich Event 2: Evidence from high-resolution stalagmite record. *Geochimica* **2006**, *35*, 586–592.
144. Liu, D.; Wang, Y.; Chen, S. DO events during 76~58 ka BP from a stalagmite in Tian'e Cave, Shennongjia area. *Acta Sedimentol. Sin.* **2007**, *25*, 131–138.
145. Dong, J.; Zhang, F. The Mid-Holcene climate variation inferred from a dated stalagmite record from Wangjiawei Cave, northeast China. *Mar. Geol. Quat. Geol.* **2012**, *32*, 119–125. [CrossRef]
146. Duan, F.; Liu, D.; Cheng, H.; Wang, X.; Wang, Y.; Kong, X.; Chen, S. A high-resolution monsoon record of millennial-scale oscillations during Late MIS 3 from Wulu Cave, south-west China. *J. Quat. Sci.* **2014**, *29*, 83–90. [CrossRef]
147. Liu, D.; Wang, Y.; Cheng, H.; Edwards, R.L.; Kong, X.; Wang, X.; Hardt, B.; Wu, J.; Chen, S.; Jiang, X. Sub-millennial variability of Asian monsoon intensity during the early MIS 3 and its analogue to the ice age terminations. *Quat. Sci. Rev.* **2010**, *29*, 1107–1115. [CrossRef]
148. Liu, D.; Wang, Y.; Cheng, H.; Edwards, R. High-resolution stalagmite $\delta^{13}C$ record of soil processes from southwestern China during the early MIS 3. *Chin. Sci. Bull.* **2013**, *58*, 796–802. [CrossRef]
149. Wang, J.; Kong, X.; Cheng, H.; Wang, Y.; Edwards, R.L. Asian summer monsoon record over 61~50 ka BP from two stalagmites from southwestern Guizhou province. *Mar. Geol. Quat. Geol.* **2008**, *28*, 85–92.
150. Tan, L.; An, Z.; Huh, C.-A.; Cai, Y.; Shen, C.-C.; Shiau, L.-J.; Yan, L.; Cheng, H.; Edwards, R.L. Cyclic precipitation variation on the western Loess Plateau of China during the past four centuries. *Sci. Rep.* **2014**, *4*, 6381. [CrossRef]
151. Tan, L.; Cai, Y.; Cheng, H.; Edwards, L.R.; Gao, Y.; Xu, H.; Zhang, H.; An, Z. Centennial-to decadal-scale monsoon precipitation variations in the upper Hanjiang River region, China over the past 6650 years. *Earth Planet. Sci. Lett.* **2018**, *482*, 580–590. [CrossRef]
152. Li, D.; Tan, L.; Cai, Y.; Jiang, X.; Ma, L.; Cheng, H.; Edwards, R.L.; Zhang, H.; Gao, Y.; An, Z. Is Chinese stalagmite $\delta^{18}O$ solely controlled by the Indian summer monsoon? *Clim. Dyn.* **2019**. [CrossRef]
153. Zhang, M.; Yuan, D.X.; Lin, Y.; Qin, J.; Bin, L.; Cheng, H.; Edwards, R.L. A 6000-year high-resolution climatic record from a stalagmite in Xiangshui Cave, Guilin, China. *Holocene* **2004**, *14*, 697–702. [CrossRef]
154. Duan, W.; Cai, B.; Tan, M.; Liu, H.; Zhang, Y. The growth mechanism of the aragonitic stalagmite laminae from Yunnan Xianren Cave, SW China revealed by cave monitoring. *Boreas* **2012**, *41*, 113–123. [CrossRef]
155. Zhang, M.; Qin, J.; Zhang, H.; Cheng, H.; Lin, Y.; Yang, Y.; Edwards, R.L.; Zhu, X. Cooling event in isotope records from a stalagmite during the middle Holcene in Xundian area, Yunnan. *Earth Environ.* **2005**, *33*, 16–22.
156. Zhang, H.; Pu, X. Stalagmite Records of Climate Change and Cold-Dry Events during the Middle Holocene in Xundian, Yunnan. *Acta Geosci. Sin.* **2011**, *32*, 95–100.
157. Zhang, M.; Lin, Y.; Zhu, X.; Qin, J.; Yang, Y.; Luo, G. The records of climatic change from a stalagmite during the late time of the middle Holocene in Ninglang area, Yunnan. *Mar. Geol. Quat. Geol.* **2006**, *26*, 35–40.
158. Che, Y.; Xiao, H.; Cui, M.; Jiang, X.; Cai, B. Timing and structure of the Heinrich 2 abrupt event inferred from a speleothem record from xianyun cave, western Fujian province. *Acta Sedimentol. Sin.* **2018**, *36*, 1139–1147.
159. Cui, M.; Xiao, H.; Sun, X.; Hong, H.; Jiang, X.; Cai, B. Characteristics of the Heinrich 1 abrupt climate event inferred from a speleothem record from Xianyun Cave, Fujian Province. *Chin. Sci. Bull.* **2017**, *62*, 3078–3088. [CrossRef]

160. Cai, Y.; An, Z.; Cheng, H.; Edwards, R.L.; Kelly, M.J.; Liu, W.; Wang, X.; Shen, C.-C. High-resolution absolute-dated Indian Monsoon record between 53 and 36 ka from Xiaobailong Cave, southwestern China. *Geology* **2006**, *34*, 621. [CrossRef]
161. Duan, W.; Cheng, H.; Tan, M.; Edwards, R.L. Onset and duration of transitions into Greenland Interstadials 15.2 and 14 in Northern China constrained by an annually laminated stalagmite. *Sci. Rep.* **2016**, *6*, 20844. [CrossRef]
162. Li, P.; Zhang, M.; Kong, X.; Zhang, C.; Wang, Y.; Zhao, K. A stalagmite record of East Asian summer monsoon in the last 2000 years and its correlation with historical records. *Mar. Geol. Quat. Geol.* **2010**, *30*, 201–208. [CrossRef]
163. Li, T.; Yuan, D.; Li, H.; Yang, Y.; Wang, J.; Wang, X.; Li, Y.; Qin, J.; Zhang, M.; Lin, Y. High-resolution climate variability of southwest China during 57-70 ka reflected in a stalagmite $\delta^{18}O$ record from Xinya Cave. *Sci. China Ser. D Earth Sci.* **2007**, *50*, 1202–1208. [CrossRef]
164. Li, J.-Y.; Li, H.-C.; Li, T.-Y.; Mii, H.-S.; Yu, T.-L.; Shen, C.-C.; Xu, X. High-resolution $\delta^{18}O$ and $\delta^{13}C$ records of an AMS ^{14}C and $^{230}Th/U$ dated stalagmite from Xinya Cave in Chongqing: Climate and vegetation change during the late Holocene. *Quat. Int.* **2017**, *447*, 75–88. [CrossRef]
165. Yang, Y.; Yuan, D.; Cheng, H.; Zhang, M.; Qin, J.; Lin, Y.; Zhu, X.; Edwards, R.L. Precise dating of abrupt shifts in the Asian Monsoon during the last deglaciation based on stalagmite data from Yamen Cave, Guizhou Province, China. *Sci. China Earth Sci.* **2010**, *53*, 633–641. [CrossRef]
166. Li, T.-Y.; Shen, C.-C.; Huang, L.-J.; Jiang, X.-Y.; Yang, X.-L.; Mii, H.-S.; Lee, S.-Y.; Lo, L. Stalagmite-inferred variability of the Asian summer monsoon during the penultimate glacial-interglacial period. *Clim. Past* **2014**, *10*, 1211–1219. [CrossRef]
167. Han, L.-Y.; Li, T.-Y.; Cheng, H.; Edwards, R.L.; Shen, C.-C.; Li, H.-C.; Huang, C.-X.; Li, J.-Y.; Yuan, N.; Wang, H.-B. Potential influence of temperature changes in the Southern Hemisphere on the evolution of the Asian summer monsoon during the last glacial period. *Quat. Int.* **2016**, *392*, 239–250. [CrossRef]
168. Li, T.-Y.; Han, L.-Y.; Cheng, H.; Edwards, R.L.; Shen, C.-C.; Li, H.-C.; Li, J.-Y.; Huang, C.-X.; Zhang, T.-T.; Zhao, X. Evolution of the Asian summer monsoon during Dansgaard/Oeschger events 13–17 recorded in a stalagmite constrained by high-precision chronology from southwest China. *Quat. Res.* **2017**, *88*, 121–128. [CrossRef]
169. Zhang, T.-T.; Li, T.-Y.; Cheng, H.; Edwards, R.L.; Shen, C.-C.; Spötl, C.; Li, H.-C.; Han, L.-Y.; Li, J.-Y.; Huang, C.-X. Stalagmite-inferred centennial variability of the Asian summer monsoon in southwest China between 58 and 79 ka BP. *Quat. Sci. Rev.* **2017**, *160*, 1–12. [CrossRef]
170. Huang, F.; Yang, X.; Lv, C.H.; Li, C.; Zhang, Y. A high-resolution stalagmite $\delta^{13}C$ record about 65-90 ka BP from Yangzi cave Chongqing. *Southwest Univ. (Nat. Sci. Ed.)* **2014**, *36*, 166–173.
171. Sun, X.; Yang, X.; Shi, Z.; Cui, G.; Fang, M.; Wang, B. The evolution of summer monsoon in Southwest China during MIS 4 as revealed by stalagmite $\delta^{18}O$ record. *Quat. Sci.* **2017**, *37*, 1370–1380.
172. Zhao, M.; Li, H.-C.; Shen, C.-C.; Kang, S.-C.; Chou, C.-Y. $\delta^{18}O$, $\delta^{13}C$, elemental content and depositional features of a stalagmite from Yelang Cave reflecting climate and vegetation changes since late Pleistocene in central Guizhou, China. *Quat. Int.* **2016**, *452*, 102–115. [CrossRef]
173. Chen, S.; Wang, Y.; Cheng, H.; Edwards, R.L.; Wang, X.; Kong, X.; Liu, D. Strong coupling of Asian Monsoon and Antarctic climates on sub-orbital timescales. *Sci. Rep.* **2016**, *6*, 32995. [CrossRef] [PubMed]
174. Zhao, K.; Chen, S.; Cui, Y.; Wang, Y.; Cheng, H. East Asian monsoon changes and its ENSO response revealed by a 200-year stalagmite record from Yongxing Cave on the Mountain Shengnonjia. *Geogr. Res.* **2015**, *34*, 74–84.
175. Liu, D.; Wang, Y.; Chen, S.; Cheng, H.; Edwards, R.L. Sub-dansgaard-oeschger events of East Asian monsoon and their global significance. *Quat. Sci.* **2008**, *28*, 169–176.
176. Liang, Y.; Chen, S.; Zhang, Z.; Yang, S.; Li, M.; Cheng, H.; Wang, Y. Abrupt monsoonal shifts over the precessional cycles documented in Yongxing Cave in China during the antepenultimate glacial period. *Environ. Earth Sci.* **2018**, *77*, 228. [CrossRef]
177. Jiang, X.; Wang, Y.; Kong, X.; Chen, S.; Li, M.; Cheng, H. Climate Variability in Shennongjia during the Last Interglacial Inferred from a High-resolution Stalagmite Record. *Acta Sedimentol. Sin.* **2008**, *26*, 139–143.
178. Jiang, X.; Li, Z.; Li, J.; Kong, X.; Guo, Y. Stalagmite $\delta^{18}O$ record from yunhua cave over the past 500 years and its regional climate significance. *Sci. Geogr. Sin.* **2012**, *32*, 207–212.

179. Huang, W.; Wang, Y.; Cheng, H.; Edwards, R.L.; Shen, C.-C.; Liu, D.; Shao, Q.; Deng, C.; Zhang, Z.; Wang, Q. Multi-Scale Holocene Asian monsoon variability deduced from a twin-stalagmite record in southwestern China. *Quat. Res.* **2016**, *86*, 34–44. [CrossRef]
180. Yin, J.-J.; Li, H.-C.; Rao, Z.-G.; Shen, C.-C.; Mii, H.-S.; Pillutla, R.K.; Hu, H.-M.; Li, Y.-X.; Feng, X. Variations of monsoonal rain and vegetation during the past millennium in Tiangui Mountain, North China reflected by stalagmite $\delta^{18}O$ and $\delta^{13}C$ records from Zhenzhu Cave. *Quat. Int.* **2017**, *447*, 89–101. [CrossRef]
181. Maher, B.A. Holocene variability of the East Asian summer monsoon from Chinese cave records: A re-assessment. *Holocene* **2008**, *18*, 861–866. [CrossRef]
182. Maher, B.A. Palaeoclimatic records of the loess/palaeosol sequences of the Chinese Loess Plateau. *Quat. Sci. Rev.* **2016**, *154*, 23–84. [CrossRef]
183. Dayem, K.E.; Molnar, P.; Battisti, D.S.; Roe, G.H. Lessons learned from oxygen isotopes in modern precipitation applied to interpretation of speleothem records of paleoclimate from Eastern Asia. *Earth Planet. Sci. Lett.* **2010**, *295*, 219–230. [CrossRef]
184. Clemens, S.C.; Prell, W.L.; Sun, Y. Orbital-scale timing and mechanisms driving Late Pleistocene Indo-Asian summer monsoons: Reinterpreting cave speleothem $\delta^{18}O$. *Paleoceanography* **2010**, *25*, PA4207. [CrossRef]
185. Clemens, S.; Holbourn, A.; Kubota, Y.; Lee, K.; Liu, Z.; Chen, G.; Nelson, A.; Fox-Kemper, B. Precession-band variance missing from East Asian monsoon runoff. *Nat. Commun.* **2018**, *9*, 3364. [CrossRef] [PubMed]
186. Pausata, F.S.; Battisti, D.S.; Nisancioglu, K.H.; Bitz, C.M. Chinese stalagmite $\delta^{18}O$ controlled by changes in the Indian monsoon during a simulated Heinrich event. *Nat. Geosci.* **2011**, *4*, 474. [CrossRef]
187. Caley, T.; Roche, D.M.; Renssen, H. Orbital Asian summer monsoon dynamics revealed using an isotope-enabled global climate model. *Nat. Commun.* **2014**, *5*, 5371. [CrossRef] [PubMed]
188. Chen, F.; Xu, Q.; Chen, J.; Birks, H.J.B.; Liu, J.; Zhang, S.; Jin, L.; An, C.; Telford, R.J.; Cao, X. East Asian summer monsoon precipitation variability since the last deglaciation. *Sci. Rep.* **2015**, *5*, 11186. [CrossRef]
189. Liu, J.; Chen, J.; Zhang, X.; Li, Y.; Rao, Z.; Chen, F. Holocene East Asian summer monsoon records in Northern China and their inconsistency with Chinese stalagmite $\delta^{18}O$ records. *Earth Sci. Rev.* **2015**, *148*, 194–208. [CrossRef]
190. Rao, Z.; Liu, X.; Hua, H.; Gao, Y.; Chen, F. Evolving history of the East Asian summer monsoon intensity during the MIS5: Inconsistent records from Chinese stalagmites and loess deposits. *Environ. Earth Sci.* **2015**, *73*, 3937–3950. [CrossRef]
191. Kutzbach, J.E. Monsoon Climate of the Early Holocene: Climate Experiment with the Earth's Orbital Parameters for 9000 Years Ago. *Science* **1981**, *214*, 59–61. [CrossRef]
192. Baker, A.J.; Sodemann, H.; Baldini, J.U.; Breitenbach, S.F.; Johnson, K.R.; Hunen, J.; Zhang, P. Seasonality of westerly moisture transport in the East Asian summer monsoon and its implications for interpreting precipitation $\delta^{18}O$. *J. Geophys. Res. Atmos.* **2015**, *120*, 5850–5862. [CrossRef]
193. Chen, J.; Rao, Z.; Liu, J.; Huang, W.; Feng, S.; Dong, G.; Hu, Y.; Xu, Q.; Chen, F. On the timing of the East Asian summer monsoon maximum during the Holocene—Does the speleothem oxygen isotope record reflect monsoon rainfall variability? *Sci. China Earth Sci.* **2016**, *59*, 2328–2338. [CrossRef]
194. Liu, Z.; Lu, Z.; Wen, X.; Otto-Bliesner, B.; Timmermann, A.; Cobb, K. Evolution and forcing mechanisms of El Niño over the past 21,000 years. *Nature* **2014**, *515*, 550–553. [CrossRef] [PubMed]
195. LeGrande, A.; Schmidt, G. Sources of Holocene variability of oxygen isotopes in paleoclimate archives. *Clim. Past* **2009**, *5*, 441–455. [CrossRef]
196. Cheng, H.; Spötl, C.; Breitenbach, S.F.; Sinha, A.; Wassenburg, J.A.; Jochum, K.P.; Scholz, D.; Li, X.; Yi, L.; Peng, Y. Climate variations of Central Asia on orbital to millennial timescales. *Sci. Rep.* **2016**, *5*. [CrossRef] [PubMed]
197. Li, X.; Liu, X.; Qiu, L.; An, Z.; Yin, Z.Y. Transient simulation of orbital-scale precipitation variation in monsoonal East Asia and arid central Asia during the last 150 ka. *J. Geophys. Res. Atmos.* **2013**, *118*, 7481–7488. [CrossRef]
198. Kutzbach, J.; Liu, X.; Liu, Z.; Chen, G. Simulation of the evolutionary response of global summer monsoons to orbital forcing over the past 280,000 years. *Clim. Dyn.* **2008**, *30*, 567–579. [CrossRef]
199. Liu, J.; Zhang, P.; Cheng, H.; Chen, F.; Yang, X.; Zhang, D.; Zhou, J.; Jia, J.; An, C.; Sang, W.; et al. Asian summer monsoon precipitation recorded by stalagmite oxygen isotopic composition in the western Loess Plateau during AD1875-2003 and its linkage with ocean-atmosphere system. *Chin. Sci. Bull.* **2008**, *53*, 2041–2049. [CrossRef]

200. Tan, L.; Cai, Y.; An, Z.; Cheng, H.; Shen, C.-C.; Gao, Y.; Edwards, R.L. Decreasing monsoon precipitation in southwest China during the last 240 years associated with the warming of tropical ocean. *Clim. Dyn.* **2017**, *48*, 1769–1778. [CrossRef]
201. He, L.; Hu, C.; Huang, J.; Xie, S.; Wang, Y. Characteristics of largescale circulation of east asian monsoon indicated by oxygen isotope of stalagmites. *Quat. Sci.* **2009**, *29*, 950–956.
202. Tan, M. Circulation effect: Climatic significance of the short term variability of the oxygen isotopes in stalagmites. *Quat. Sci.* **2009**, *29*, 851–862.
203. Tan, M. Circulation effect: Response of precipitation $\delta^{18}O$ to the ENSO cycle in monsoon regions of China. *Clim. Dyn.* **2014**, *42*, 1067–1077. [CrossRef]
204. Tan, M. Circulation background of climate patterns in the past millennium: Uncertainty analysis and re-reconstruction of ENSO-like state. *Sci. China Earth Sci.* **2016**, *59*, 1225–1241. [CrossRef]
205. Zhang, H.; Cheng, H.; Cai, Y.; Spötl, C.; Sinha, A. Effect of precipitation seasonality on annual oxygen isotopic composition in the area of spring persistent rain in Southeastern China and its palaeoclimatic implication. *Clim. Past Discuss.* **2018**, *2018*, 1–22. [CrossRef]
206. Berger, A. Long-term variations of caloric insolation resulting from the Earth's orbital elements. *Quat. Res.* **1978**, *9*, 139–167. [CrossRef]
207. Bereiter, B.; Eggleston, S.; Schmitt, J.; Nehrbass-Ahles, C.; Stocker, T.F.; Fischer, H.; Kipfstuhl, S.; Chappellaz, J. Revision of the EPICA Dome C CO_2 record from 800 to 600 kyr before present. *Geophys. Res. Lett.* **2015**, *42*, 542–549. [CrossRef]
208. Spratt, R.M.; Lisiecki, L.E. A Late Pleistocene sea level stack. *Clim. Past* **2016**, *12*, 1079–1092. [CrossRef]
209. Hays, J.D.; Imbrie, J.; Shackleton, N.J. Variations in the Earth's orbit: Pacemaker of the ice ages. *Science* **1976**, *194*, 1121–1132. [CrossRef]
210. Chiang, J.; Swenson, L.; Kong, W. Role of seasonal transitions and the westerlies in the interannual variability of the East Asian summer monsoon precipitation. *Geophys. Res. Lett.* **2017**, *44*. [CrossRef]
211. Li, Y.; Rao, Z.; Cao, J.; Jiang, H.; Gao, Y. Highly negative oxygen isotopes in precipitation in southwest China and their significance in paleoclimatic studies. *Quat. Int.* **2016**, *440*, 64–71. [CrossRef]
212. Maher, B.A.; Thompson, R. Oxygen isotopes from Chinese caves: Records not of monsoon rainfall but of circulation regime. *J. Quat. Sci.* **2012**, *27*, 615–624. [CrossRef]
213. Kathayat, G.; Cheng, H.; Sinha, A.; Spötl, C.; Edwards, R.L.; Zhang, H.; Li, X.; Yi, L.; Ning, Y.; Cai, Y. Indian monsoon variability on millennial-orbital timescales. *Sci. Rep.* **2016**, *6*, 24374. [CrossRef] [PubMed]
214. Dansgaard, W.; Johnsen, S.; Clausen, H.; Dahl-Jensen, D.; Gundestrup, N.; Hammer, C.; Hvidberg, C.; Steffensen, J.; Sveinbjörnsdottir, A.; Jouzel, J. Evidence for general instability of past climate from a 250-kyr ice-core record. *Nature* **1993**, *364*, 218. [CrossRef]
215. Peterson, L.C.; Haug, G.H.; Hughen, K.A.; Röhl, U. Rapid changes in the hydrologic cycle of the tropical Atlantic during the last glacial. *Science* **2000**, *290*, 1947–1951. [CrossRef] [PubMed]
216. Zhou, H.; Zhao, J.; Zhang, P.; Shen, C.-C.; Chi, B.; Feng, Y.; Lin, Y.; Guan, H.; You, C.-F. Decoupling of stalagmite-derived Asian summer monsoon records from North Atlantic temperature change during marine oxygen isotope stage 5d. *Quat. Res.* **2008**, *70*, 315–321. [CrossRef]
217. Broecker, W.S. Paleocean circulation during the last deglaciation: A bipolar seesaw? *Paleoceanography* **1998**, *13*, 119–121. [CrossRef]
218. Stocker, T.F.; Johnsen, S.J. A minimum thermodynamic model for the bipolar seesaw. *Paleoceanography* **2003**, *18*, 1078. [CrossRef]
219. Rasmussen, S.O.; Andersen, K.K.; Svensson, A.; Steffensen, J.P.; Vinther, B.M.; Clausen, H.B.; Siggaard-Andersen, M.L.; Johnsen, S.J.; Larsen, L.B.; Dahl-Jensen, D. A new Greenland ice core chronology for the last glacial termination. *J. Geophys. Res. Atmos.* **2006**, *111*, D06102. [CrossRef]
220. Members, W.D.P.; Buizert, C.; Adrian, B.; Ahn, J.; Albert, M.; Alley, R.B.; Baggenstos, D.; Bauska, T.K.; Bay, R.C.; Bencivengo, B.B.; et al. Precise interpolar phasing of abrupt climate change during the last ice age. *Nature* **2015**, *520*, 661. [CrossRef]
221. Stuiver, M.; Grootes, P.M. GISP2 oxygen isotope ratios. *Quat. Res.* **2000**, *53*, 277–284. [CrossRef]
222. Cosford, J.; Qing, H.; Eglington, B.; Mattey, D.; Yuan, D.; Zhang, M.; Cheng, H. East Asian monsoon variability since the Mid-Holocene recorded in a high-resolution, absolute-dated aragonite speleothem from Eastern China. *Earth Planet. Sci. Lett.* **2008**, *275*, 296–307. [CrossRef]

223. Tan, M.; Cai, B. Preliminary calibration of stalagmite oxygen isotopes from Eastern Monsoon China with Northern Hemisphere temperatures. *Pages News* **2005**, *13*, 16–17. [CrossRef]
224. Yang, X.; Yang, H.; Wang, B.; Huang, L.-J.; Shen, C.-C.; Edwards, R.L.; Cheng, H. Early-Holocene monsoon instability and climatic optimum recorded by Chinese stalagmites. *Holocene* **2019**, *29*, 1059–1067. [CrossRef]
225. Mudelsee, M. Ramp function regression: A tool for quantifying climate transitions. *Comput. Geosci.* **2000**, *26*, 293–307. [CrossRef]
226. Liu, Y.; Hu, C. Quantification of southwest China rainfall during the 8.2 ka BP event with response to North Atlantic cooling. *Clim. Past* **2016**, *12*, 1583–1590. [CrossRef]
227. Jin, G.; Liu, D. Mid-Holocene climate change in North China, and the effect on cultural development. *Chin. Sci. Bull.* **2002**, *47*, 408–413. [CrossRef]
228. Cheng, H.; Fleitmann, D.; Edwards, R.L.; Wang, X.; Cruz, F.W.; Auler, A.S.; Mangini, A.; Wang, Y.; Kong, X.; Burns, S.J. Timing and structure of the 8.2 kyr BP event inferred from $\delta^{18}O$ records of stalagmites from China, Oman, and Brazil. *Geology* **2009**, *37*, 1007. [CrossRef]
229. Perșoiu, A.; Ionita, M.; Weiss, H. Atmospheric blocking induced by the strengthened Siberian High led to drying in west Asia during the 4.2 ka BP event—A hypothesis. *Clim. Past* **2019**, *15*, 781–793.
230. Berkelhammer, M.; Sinha, A.; Stott, L.; Cheng, H.; Pausata, F.S.; Yoshimura, K. An abrupt shift in the Indian monsoon 4000 years ago. *Geophys. Monogr. Ser* **2012**, *198*, 75–87.
231. Bond, G.; Kromer, B.; Beer, J.; Muscheler, R.; Evans, M.N.; Showers, W.; Hoffmann, S.; Lotti-Bond, R.; Hajdas, I.; Bonani, G. Persistent solar influence on North Atlantic climate during the Holocene. *Science* **2001**, *294*, 2130–2136. [CrossRef]
232. Yin, J.; Qin, J.; Lin, Y.; Yang, Y.; Tang, W. Research progress on the recent 2000 years' climate change revealed by stalagmite record in China. *Carsologica Sin.* **2010**, *29*, 258–266.
233. Li, C.; Ku, T.; Dorte, P.; Wang, F.; Chen, W.; Yin, G.; Cheng, H.; Edwards, R.L. Paleoclimatic and paleomonsoonal variations in central china recorded by stable isotopic records of stalagmites from Buddha cave, South Shaanxi. *Seismol. Geol.* **2000**, *22*, 63–78.
234. Zhang, C.; Zhang, M.; Li, P.; Kong, X.; Zhu, Z.; Jiang, X.; Wang, Y. Stalagmite $\delta^{18}O$ record 2592-1225 yr BP from Mt. Shennongjia and its regional climate significance. *Sci. Geogr. Sinca* **2010**, *30*, 950–954.
235. Tan, L.; Cai, Y.; Cheng, H.; Edwards, L.R.; Lan, J.; Zhang, H.; Li, D.; Ma, L.; Zhao, P.; Gao, Y. High resolution monsoon precipitation changes on Southeastern Tibetan Plateau over the past 2300 years. *Quat. Sci. Rev.* **2018**, *195*, 122–132. [CrossRef]
236. Moberg, A.; Sonechkin, D.M.; Holmgren, K.; Datsenko, N.M.; Karlén, W. Highly variable Northern Hemisphere temperatures reconstructed from low-and high-resolution proxy data. *Nature* **2005**, *433*, 613. [CrossRef] [PubMed]
237. Knudsen, M.F.; Riisager, P.; Jacobsen, B.H.; Muscheler, R.; Snowball, I.; Seidenkrantz, M.S. Taking the pulse of the Sun during the Holocene by joint analysis of ^{14}C and ^{10}Be. *Geophys. Res. Lett.* **2009**, *36*. [CrossRef]
238. Perry, C.A.; Hsu, K.J. Geophysical, archaeological, and historical evidence support a solar-output model for climate change. *Proc. Natl. Acad. Sci. USA* **2000**, *97*, 12433–12438. [CrossRef] [PubMed]
239. Mann, M.E.; Zhang, Z.; Rutherford, S.; Bradley, R.S.; Hughes, M.K.; Shindell, D.; Ammann, C.; Faluvegi, G.; Ni, F. Global signatures and dynamical origins of the Little Ice Age and Medieval Climate Anomaly. *Science* **2009**, *326*, 1256. [CrossRef]
240. Yang, H.; Johnson, K.; Griffiths, M.; Yoshimura, K. Interannual controls on oxygen isotope variability in Asian monsoon precipitation and implications for paleoclimate reconstructions. *J. Geophys. Res. Atmos.* **2016**, *121*, 8410–8428. [CrossRef]
241. Yan, H.; Sun, L.; Wang, Y.; Huang, W.; Qiu, S.; Yang, C. A record of the Southern Oscillation Index for the past 2000 years from precipitation proxies. *Nat. Geosci.* **2011**, *4*, 611. [CrossRef]
242. Lean, J.L.; Wang, Y.M.; Sheeley, N. The effect of increasing solar activity on the Sun's total and open magnetic flux during multiple cycles: Implications for solar forcing of climate. *Geophys. Res. Lett.* **2002**, *29*, 71. [CrossRef]
243. Li, W.; Li, L.; Ting, M.; Liu, Y. Intensification of Northern Hemisphere subtropical highs in a warming climate. *Nat. Geosci.* **2012**, *5*, 830. [CrossRef]
244. Change, I.C. Synthesis Report Summary for Policymakers. 2014. Available online: https://www.ipcc.ch/pdf/assessment-report/ar5/syr/AR5_SYR_FINAL_SPM.pdf (accessed on 10 July 2019).

245. Li, Z.; Lau, W.M.; Ramanathan, V.; Wu, G.; Ding, Y.; Manoj, M.; Liu, J.; Qian, Y.; Li, J.; Zhou, T. Aerosol and monsoon climate interactions over Asia. *Rev. Geophys.* **2016**, *54*, 866–929. [CrossRef]
246. Tan, L.; Cai, Y.; Cheng, H.; Edwards, R.L.; Shen, C.-C.; Gao, Y.; An, Z. Climate significance of speleothem $\delta^{18}O$ from central China on decadal timescale. *J. Asian Earth Sci.* **2015**, *106*, 15. [CrossRef]